20

Processing nanostructured metal and metal-matrix coatings by thermal and cold spraying

G.E. KIM, Perpetual Technologies Inc., Canada, V.K. CHAMPAGNE and M. TREXLER, US Army Research Laboratory AMSRD-ARL-WM-MC, USA and Y. SOHN, University of Central Florida, USA

Abstract: This chapter provides an overview of the development and application of nanostructured coatings, with an emphasis on the latest results on metal-base materials. Thermal spray processing of nanostructured ceramic coatings have been successfully implemented in Navy and industrial applications. Thermal and cold spray processes have been used to deposit dense, oxide-free nanostructured coatings from metal-base feedstock. Different approaches for manufacturing nanostructured metal and metal-matrix composite feedstocks have been presented. Thermal and cold spraying of nanostructured metal-base coatings show promise in better protecting components that are exposed to high temperatures, to corrosion, and to wear.

Key words: metal-base coatings, nanostructured, cold spray, thermal spray, HVOF.

20.1 Introduction

This chapter provides an overview of the development and application of nanostructured metal-base coatings. The search for improved wear and corrosion-resistant coatings has recently focused on developing nanostructured materials such as alumina-titania and tungsten carbide-cobalt. Applications that may benefit from nanostructured metal-base coatings include oxidation and hot corrosion-resistant alloys, electronics, bioengineering and anti-fretting applications.

To incorporate metal-base nanostructured coatings on a commercial scale, a cost-effective, scaleable powder feedstock processing method is required. Amongst several approaches for the processing of nanostructured powder, non-cryogenic milling (NCM) has recently emerged as a promising option. Non-cryogenic milling can process larger quantities of metal-base powder in a relatively short duration, at a lower cost than competing processes.

The use of nanostructured coatings also requires an appropriate method of application. Starting with the first research in this area in 1997 at the United States Office of Naval Research (ONR),[1] thermal spray processes have been successfully used to deposit nanostructured coatings of metals, ceramics, and their composites. A range of these coatings is reviewed in this chapter.

When spraying nanostructured coatings, there are particular requirements in preserving the functionality of the feedstock powder in the final coating. This is especially true when depositing temperature sensitive and readily oxidizing materials such as carbides, nitrides, and metals. For these materials, the goal is to replace most, if not all, of the thermal energy (i.e. flame temperature) with kinetic energy (i.e. particle velocity) so as to retain the nanostructure without contributing to coating oxidation or porosity. The introduction of a relatively new deposition process, referred to as the cold spray process, is particularly suited to meet the low-temperature, high-velocity criteria for the deposition of dense, oxide-free metal-base nanostructured coatings. The cold spray process demonstrates the ability to deposit dense, oxide-free, nanostructured aluminum alloy coating that may improve resistance against localized corrosion and wear. In addition to coatings applications, the same approach may be further developed to spray-form nanostructured metal-base components. Cold spray of nanostructured metal-base materials may also contribute to stronger near net-shape spray nanostructured forms, and better repair of worn/damaged components.

This chapter reviews key developments in the manufacture of nanostructured metal-base feedstock, including high-energy ball milling (HEM), the use of cryomilling and the development of new techniques that do not require the use of liquid nitrogen. It goes on to discuss the use of thermal spray techniques for applying a broad range of coatings and the application of the cold spray process to more sensitive materials as a way of achieving coatings with the required functionality.

20.2 Nanostructured metal-base feedstock

As with the processing of bulk nanomaterials and nanoparticles, the processing of nanostructured powders can be top-down, bottom-up, and a combination of the two. In the top-down approach, nanostructured powders can be produced by refining coarse-grained materials. A common top-down approach is via severe plastic deformation (SPD) techniques such as ball milling. In the bottom-up approach, nanostructured particles can be assembled from atoms, molecules and/or nanoparticles. An example of the bottom-up approach to forming nanostructured powder is the spray drying of nanoparticles.

High-energy ball milling (HEM) is a commercially available, relatively low-cost approach that has been fairly widely used to produce nanostructured powder.[2,3,4] There are numerous types of HEM systems, including shaker mills, Simoloyer® high-energy mills, planetary grinding mills, vertical attritors, and drum mills. In addition to microstructure refinement of metal-base powder, the very high energy transfer of HEM systems can be used to activate chemical reactions (i.e. reactive milling, mechanical alloying), to reduce particle size of hard and brittle materials, and to produce metal matrix composite (MMC) powder with uniformly distributed reinforcing particles within a very fine metal matrix. In

addition to its relatively low cost, HEM systems are scalable to meet commercial demands.

When working with relatively ductile and elastic materials like many metals, milling in cryogenic temperatures (cryomilling) embrittles the powder, making it grindable. In addition, the extremely low temperature suppresses recovery and recrystallization, thereby resulting in finer grain structure. In addition to rapid grain refinement, the liquid nitrogen environment serves to mitigate oxidation, promote fracturing, and form nanodispersoids of nitrides and/or oxy-nitrides within the metal powder. The latter helps strengthen the metal matrix.

It is important to note, however, that cryomilling is not economically viable for commercial applications in many cases due to the high cost of liquid nitrogen. In 2003, n-WERKZ Inc was created to focus on developing a new approach to processing nanostructured metal-base powders with the potential for larger scale production and at competitive costs. A study carried out by Ye *et al*.[5] provides an insight into the high cost associated with the need for liquid nitrogen when cryomilling metal powders into nanostructure form.

In 2003, n-WERKZ received partial funding from ONR to study the feasibility of processing AA5083 (Al 4.0-4.9 Mg 0.4-1.0 Mn 0.4 Si 0.4 Fe 0.25 Zn 0.15 Ti 0.1 Cu 0.05-0.25 Cr in wt%) and NiCrAlY powders into nanostructure form without the use of liquid nitrogen. After three and a half years of experimentation, a new design and fabrication of customized equipment finally led to the successful processing of nanostructured metal powders with equiaxed particles. The general approach to compensating for the absence of liquid nitrogen was to increase the strain rate exerted onto the particles during milling. Details of the customized equipment and the processing parameters are confidential to n-WERKZ Inc. The company has disclosed that, even without the use of liquid nitrogen in their processing, the milling time is shorter than cryomilling for similar powder characteristics.

The spray drying of nanoparticles to form oral drug delivery systems has also been developed successfully.[6,7] A similar approach has been successfully used for processing nanostructured ceramic powders, which were then used to deposit thermal sprayed nanostructured ceramic coatings.[8,9] Figure 20.1 shows a scanning electron microscope (SEM) view of a spray-dried nanostructured TiO_2 particle from Altair (Reno, Nevada) used to deposit a nanostructured coating. Spray drying has also been used to agglomerate nanoparticles of WC with Co as shown in Fig. 20.2.[10] Agglomerates of metal nanoparticles have also been spray dried.

20.3 Thermal spray processing

Thermal spray is by far the most versatile modern surfacing method in terms of economics, range of materials, and scope of applications. It consists of projecting molten or semi-molten particles of metals, ceramics, or their composites from powder, solution/suspension, or wire feedstock (Fig. 20.3).[11] A general rule of

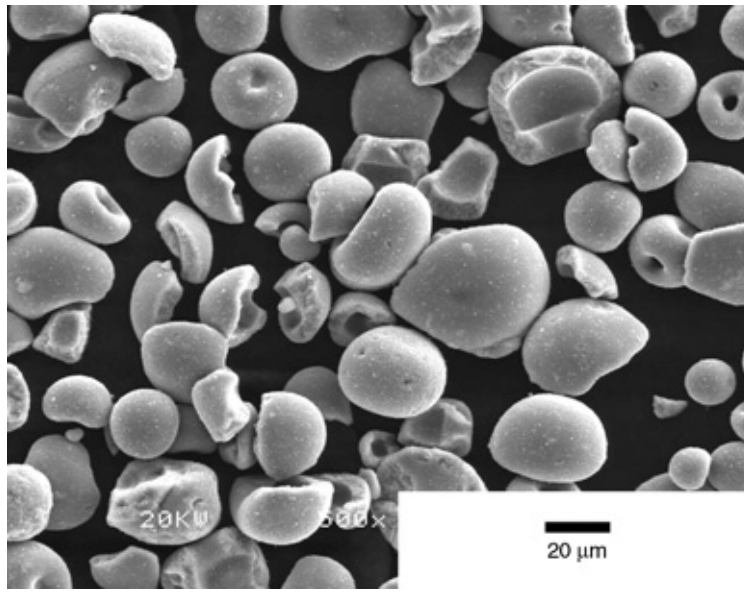

20.1 Spray-dried nanostructured TiO_2 particle from Altair.

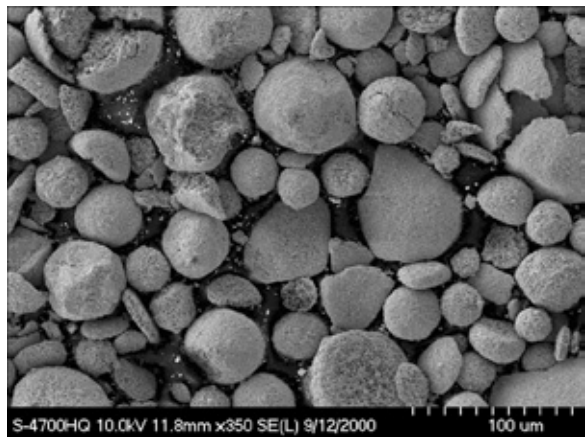

20.2 Agglomerated nanostructured WC-12Co powder.

thumb is that any material that has a stable molten phase and can be processed into the appropriate feed specifications can be thermal sprayed. The heat source used to heat and accelerate the feedstock is generated either chemically via oxygen-fuel combustion, or electrically via an arc.

The hot molten or semi-molten particles impinge and solidify on the surface forming a layered, lamellar structure. Depending on the desired thickness of the deposit, single or multiple passes of the torch at any given region can be carried

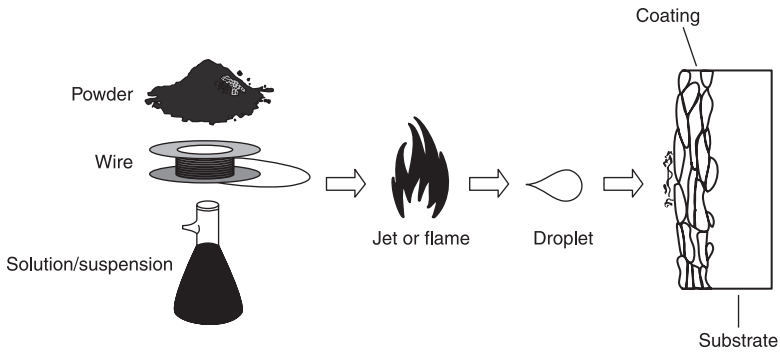

20.3 Agglomerated nanostructured WC-12Co powder.

out. A typical thermal sprayed monolithic coating will consist of inherent non-homogeneous features, including very fine grains, splat boundaries, pores, oxide inclusions, and partially melted or unmelted particles. Even with this non-homogeneous structure, a well-applied thermal spray coating will provide reliable protection against many wear, corrosion and thermal conditions. It is important to note, however, that thermal sprayed coatings are not often used as a corrosion barrier without the aid of a sealant.

Each thermal spray process has a unique combination of requirements and capabilities. The most important requirements are generally the type of feedstock material (e.g. powder, solution/suspension, or wire) and the type of energy source (e.g. liquid fuel or electricity). In addition, factors such as the melting temperature of the feedstock, the type of substrate, the particle size distribution, the target microstructure of the coating (e.g. porosity, grain size, chemistry, oxide content), and the available budget, can be useful in narrowing the spectrum of thermal spray processes that may be appropriate for a given application.

In working with nanostructured metal-base materials to produce a coating, the process requirements and capabilities are quite particular. Typically, the desired coating is dense, with low thermal degradation (e.g. oxidation, decarburization) and limited grain growth. In addition, although there are different forms of attainable nanostructured metal-base feedstock, nanostructured powders seem to have the best combination of characteristics to produce a good final coating.

In terms of capabilities, thermal spray processes may be differentiated from one another by focusing on two main parameters:

- the typical flame temperature;
- particle velocity.

Out of all the types of thermal spray processes available, the High-Velocity OxyFuel (HVOF) process has made a significant impact in the application of metal-base coatings. As with other combustion spray processes, the HVOF

process uses liquid fuel. However, its torch design incorporates a nozzle that dramatically increases gas acceleration. The combination of high gas velocities in the range of 1500 to 2000 m/s and relatively low gas temperatures in the order of 3000°C is ideal for depositing temperature-sensitive, dense coatings. A large proportion of HVOF applications are for temperature-sensitive carbide composites such as WC-Co and Cr_3C_2-NiCr. The process capabilities that make HVOF ideal for spraying carbides – namely high velocities at reduced temperatures – are also beneficial for spraying nanostructured metal-base coatings. An operating HVOF is presented in Fig. 20.4.[12]

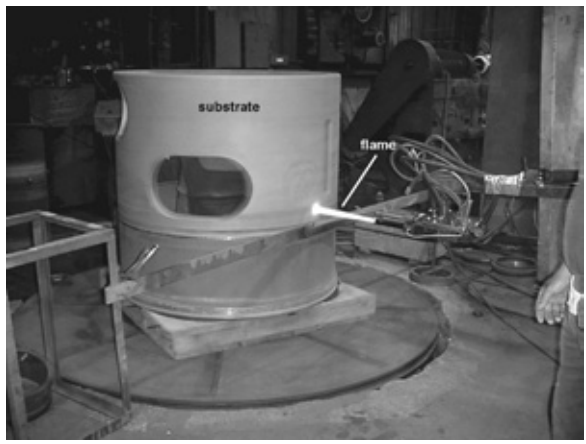

20.4 Operating high velocity oxyfuel system.

20.4 Thermal spray processing of nanostructured coatings: tungsten carbide-cobalt (WC-Co) coatings

Results from research carried out by different institutions on thermal sprayed nanostructured WC-Co coatings have lacked reproducibility and did not show any clear advantage over conventional WC-Co coatings.[13–15] This seems to have been due to variations in the parameters for thermal spray processing by each applicator, and to the susceptibility of the carbide nanoparticle within the cobalt matrix to undergoing accelerated and extensive decarburization. There are, however, several studies that show favorable wear, microhardness, fatigue, and corrosion results for nanostructured WC-base coatings when compared directly to conventional coatings of the same composition.[16–22]

The US Office of Naval Research (ONR) research program has focused on the processing of nanostructured oxide and tungsten carbide-cobalt (WC-Co) coatings mainly for wear and corrosion applications. The goal was to fabricate coatings that exhibit hardness, toughness, abrasion resistance, and reduce ongoing

maintenance costs by extending the service life of ship machinery and assets. The program has been a huge success, with estimated annual cost savings approaching $100 million for the US Navy. Some of the coatings developed under this program are discussed in the following sections.

20.5 Thermal spray processing of nanostructured coatings: alumina-titania (n-AT) coatings

Research by Gell *et al*.[23,24,25] at the University of Connecticut (UCONN) within the ONR program has resulted in the development of a nanostructured alumina-titania (n-AT) coating. This novel coating has shown unique and superior properties compared to a conventional coating of the same composition. These properties included double the bond strength, up to four times the abrasive resistance, and enhanced toughness. The very favorable test results of the n-AT coating have resulted in its application on numerous Navy components. Examples of components with n-AT coating include:[26]

- titanium submarine doors bolted to steel frames and immersed in saltwater;
- ball valves that regulate water flow in submarines;
- pump components that control submarine diving and resurfacing;
- 80-ton air conditioner components on ships.

Among the numerous Navy components with the n-AT coating, one application clearly stands out as benefiting from the unique attributes of this coating. This application involves the main propulsion shafts of mine countermeasure (MCM) ships. Since modern mines are triggered not only by collision, but also by sound or magnetic signature of a ship, every effort is made to minimize the use of materials that trigger a magnetic resonance. Hence, the MCM shafts, for example, cannot be fabricated from ferrous material like steel, and are replaced by non-magnetic nickel aluminum bronze (NAB), which is considerably softer than steel. NAB shafts have suffered from excessive wear in the stern tube and bearing strut areas due to bio-growth between the bearing staves. In addition to the cost of repair for the shafts, replacing these shafts also requires dry-docking the ships. Figure 20.5 shows a dry-docked MCM and a view of the main propulsion shaft.

Due to the significant levels of torque, bending, and fatigue experienced by the shafting, conventional brittle ceramic coatings were never feasible for this application. Instead, n-AT coatings were applied by Norfolk Naval Shipyard under a NAVSEA Engineering for Reduced Maintenance project. Currently, the majority of the MCMs in the Navy Fleet operate with n-AT coated shafts. In February 2009, one of the ship sets was removed and evaluated at a Navy shipyard. After seven years in service, there were no signs of spallation resulting from wear and/or corrosion. In fact, over 80% of the coating showed no visible signs of degradation. Considering a repair cost of $75 000 per ship set with the new thermal spray of n-AT approach, compared to the former OEM repair cost of

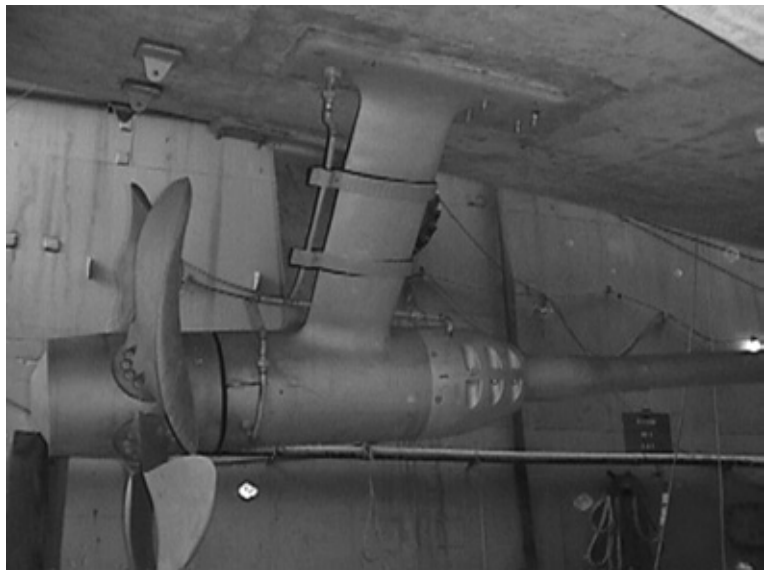

20.5 View of the main propulsion shaft region of a mine countermeasures ship.

$275 000 per ship set, this new approach is very attractive. The original estimate of return on investment cost avoidance, based on an improvement of two-fold service life with the nanostructured coating, was over $34 000 000 over the remaining life of these components for the fleet of MCMs. Latest in-service results point to a four-fold life-extension improvement, thus further increasing the return on investment by a considerable amount.

20.6 Thermal spray processing of nanostructured coatings: titanium oxide coatings

In April 2000, with the permission of the US Navy, Perpetual Technologies set out to develop thermal spray nanostructured ceramic coatings for industrial application. Within a month, a collaborative agreement with Mogas Industries and FW Gartner was established to develop a nanostructured titanium oxide (n-TiO_2) coating customized for use for severe-service ball valves. The objective was to produce a novel coating that would extend the service-life of ball valves exposed to very extreme conditions found in nickel/cobalt high-pressure acid leach (HPAL) process, including high temperatures (~265°C); high pressures (4700 to 5500 kPa); high sulfuric acid concentrations (>95%); and high solids concentrations (>20 wt%).

The choice of titanium oxide was based on the knowledge that titanium was one of the materials that show reasonable chemical resistance to this harsh environment.

The n-TiO_2 coating possessed increased hardness and superior wear resistance. Figure 20.6 provides the results of abrasion and slurry erosion tests conducted on conventional and n-TiO_2 coatings. The dramatic reduction in volume loss of the abraded n-TiO_2 coating compared to that of the conventional coating was not due solely to the increase in microhardness. It was the unique combination of increased hardness along with the increased toughness that led to this drastic enhancement in abrasive wear resistance.[27,28,29] Although the increased toughness was not measured quantitatively, numerous qualitative features validate the presence of increased toughness in the nanostructured coatings.

Common knowledge in the study of erosion states that ductile materials undergo higher erosion loss at low-impingement angles relative to the substrate surface. The opposite is true for harder materials, in that they undergo higher erosion loss at high-impingement angles. The n-TiO_2 coatings samples showed a reduction in volume loss at both high- and low-slurry impingement angles compared to the conventional coating samples. This result is unique and attributable to the nanostructured coating possessing increased hardness and toughness characteristics.

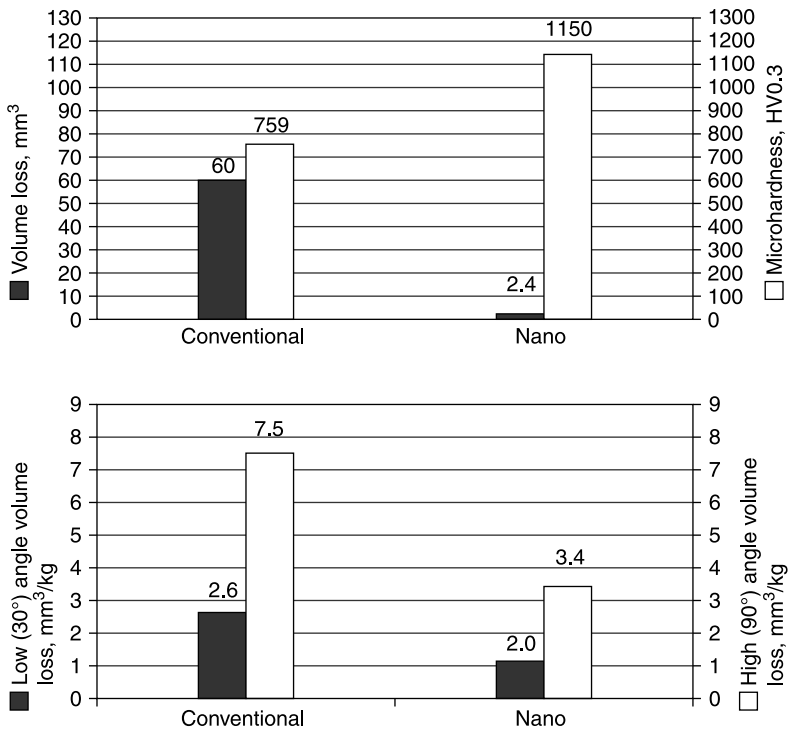

20.6 Abrasion (top) and slurry erosion (bottom) wear test results on TiO_2 coatings.

The second feature that revealed the superior toughness of n-TiO_2 coatings is shown in Fig. 20.7. This figure provides views of the indented (with 500g load) regions of each coating cross-section. It is clearly apparent that the n-TiO_2 coating had lower degrees of crack density, width, and length, as compared to the conventional coating.

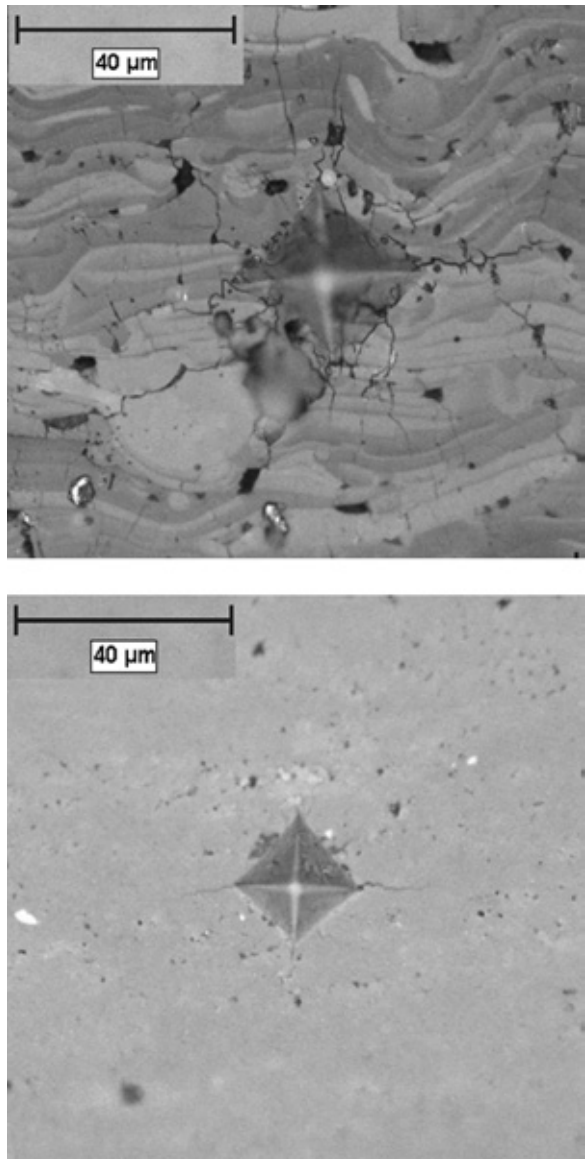

20.7 Conventional (top) and nanostructured (bottom) TiO_2 coating cross-sections following 500 g Vickers indent.

In addition to the increased toughness, i.e. resistance to crack propagation, the depth of indentation at the same load for both coatings reveals a harder nanostructured coating. Closer examination of the region around the cracks in the nanostructured coating revealed an interesting connection between the presence of nano-porous, unmelted or partially melted particles and crack propagation. These fine-pored agglomerates seemed to deflect the crack and/or blunt the crack tip, thus hindering its propagation. The same effect was not observed on dense unmelted particles found in the commercial coating.

The third feature was demonstrated by the scars left on the surface of the coatings following abrasion tests, low-impingement slurry erosion tests, and high-impingement slurry erosion tests. It was evident from SEM views of both types of coating surfaces (Fig. 20.8) that, in all three tests, the scars left on the n-TiO_2 coating were smoother

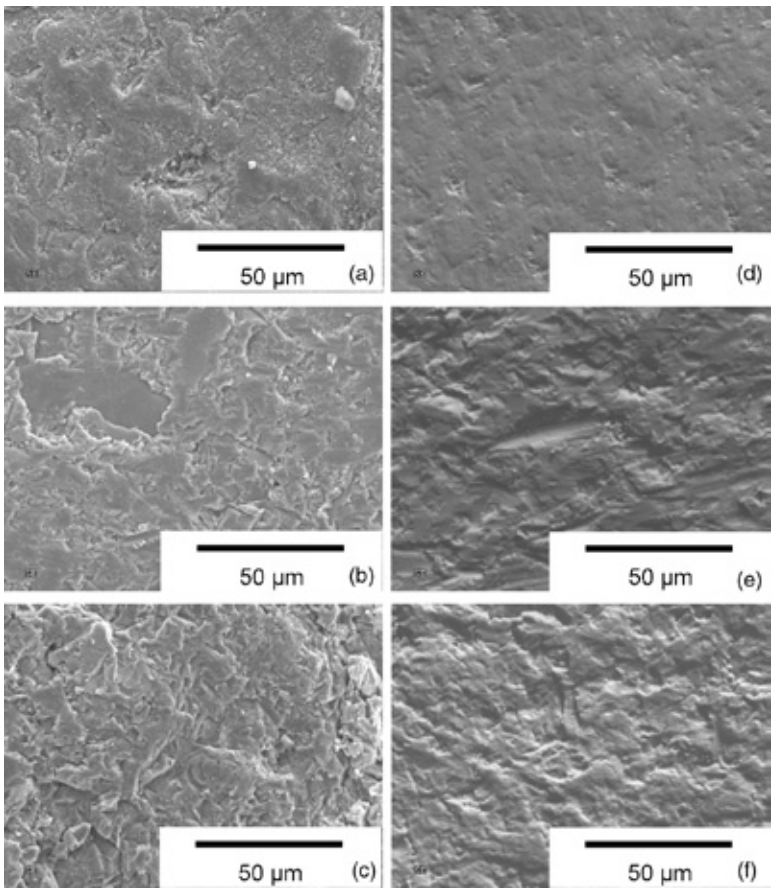

20.8 Scars on conventional TiO_2 coating following abrasion (a), low-impingement angle erosion (b), high-impingement angle erosion (c) and nanostructured TiO_2 coating following abrasion (d), low-impingement angle erosion (e), high-impingement angle erosion (f).

and possessed physical characteristics of ductile wear, i.e. microploughing, microcutting, plastic deformation, directional scarring (at low-impingement angles). On the other hand, the surfaces of the conventional samples were rougher and possessed the physical characteristics of brittle wear, i.e. microcracking, spallation (especially along the splat boundaries), very little directional scarring at low-impingement angle slurry erosion.

Based on these very promising laboratory results, the n-TiO_2 coating was first applied onto field components in late 2001. Although hundreds of ball valve components were coated with n-TiO_2 coating, it was only in 2003 that a direct comparison between n-TiO_2 and the previously incorporated coating of chromium oxide blend was carried out at Lihir mines in Papua New Guinea. Figure 20.9

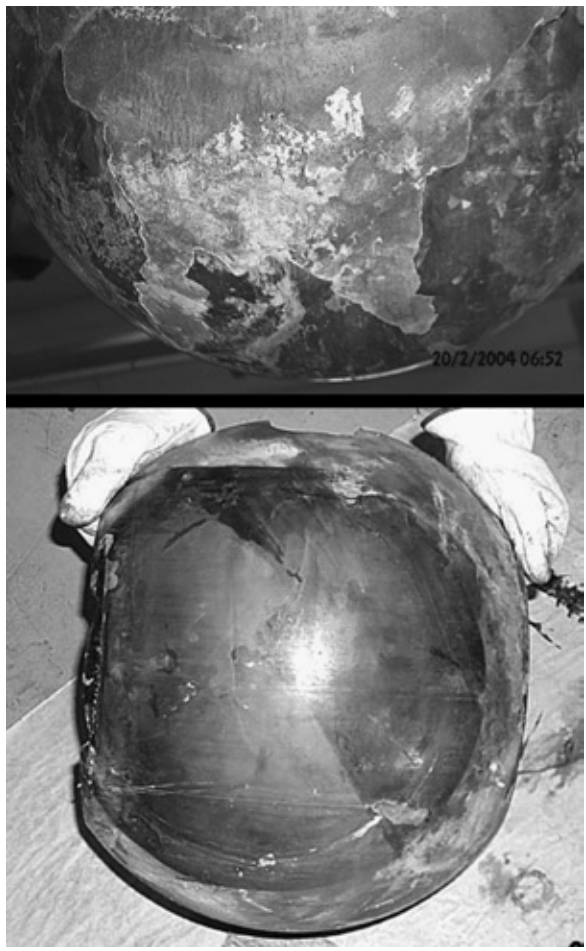

20.9 Ten-inch titanium balls with chromia-blend (top) and nanostructured (bottom) TiO_2 coatings after ten months of service.

provides photographs of the ball surface following 10 months of parallel service between two identical ten-inch valves, each with a different type of coating. It was clearly evident that the n-TiO_2 coating was in a far superior state when compared to the non-nanostructured Cr_2O_3-blend coating. The surface of Cr_2O_3-blend coated ball had large regions without coating, which led to slurry leakage. In contrast, the n-TiO_2 coated ball had a few isolated regions without coating and was returned into service without rework.

In 2007, a mine in Western Australia applied and tested the n-TiO_2 coating on lab scale impeller blades against slurry erosion. The results indicated a more than two-fold increase in coating life with the n-TiO_2 coating when compared to the coating that was being previously applied. On the basis of this result, over 46 field impeller blades have been coated with the nanostructured coating. There are currently ten or more installations around the world with n-TiO_2 coated ball valves.

20.7 Thermal spray processing of nanostructured coatings: MCrAlY and NiCrAlY coatings

In 2001, researchers at Perpetual Technologies Inc and National Institute of Standards and Technology (NIST) approached ONR with an idea to develop and study nanostructured MCrAlY bond coats for high temperature applications. The general approach was to process nanostructured MCrAlY powder using cryomilling technique, to thermal spray the powder to form nanostructured coating samples, and to evaluate the samples and compare test results to those of conventional MCrAlY coating samples. The tests were carried out with samples as single-layer MCrAlY only and as a thermal barrier coating (TBC) duo layer of MCrAlY bond coat and yttria partially stabilized zirconia (YPSZ) top coat.

20.7.1 Manufacturing MCrAlY and NiCrAlY coatings by cyromilling

In 2001, Perpetual Technologies Inc, NIST, and UCD started a three-year program to cryomill conventional MCrAlY powder to form nanostructured powder and to deposit this transformed feedstock powder into coating form using conventional thermal spray processes. NI-343 powder from Praxair (Ni-22Cr-10Al-1Y in wt%) was the first alloy studied in detail within this program.[30,31,32]

Cryomilling took place for eight hours in a Model 1-S attritor mill where the stainless steel milling media and NiCrAlY powders were submersed in liquid nitrogen.[33] The powders were characterized using X-ray diffraction (XRD), transmission electron microscopy (TEM), chemical analysis, and thermal analysis. Conventional and nanostructured NiCrAlY powders were sprayed using thermal spray techniques typically used by gas turbine engine original equipment manufacturers (OEMs). The two thermal spray processes used to deposit NiCrAlY coatings in this program were HVOF and LPPS. The coatings underwent

microhardness, nanoindentation, XRD, SEM, and TEM evaluations. Static oxidation and thermal cycling experiments were conducted on NiCrAlY-only and NiCrAlY with YPSZ top coat samples, respectively. The results for samples with nanostructured NiCrAlY coating were compared directly to those with conventional NiCrAlY coating.

Figure 20.10 provides an SEM view of the as-received, conventional and the nanostructured NiCrAlY powders. The cryomilled powder had a larger average

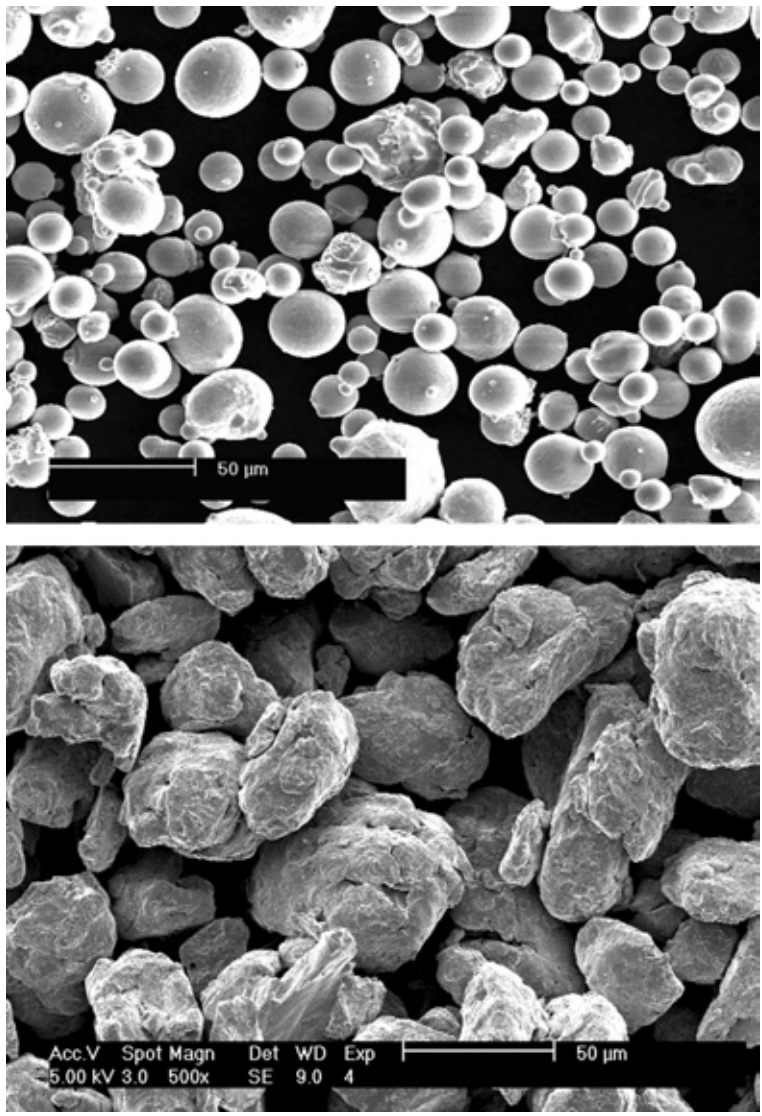

20.10 As-received conventional and cryomilled NiCrAlY powder.

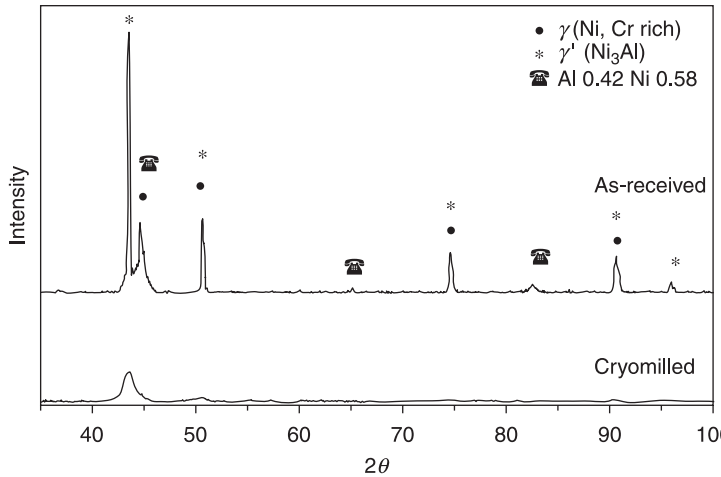

20.11 X-ray diffraction spectra for as-received and cryomilled NiCrAlY powders.

particle of about 40 μm as compared to about 21 μm for the conventional powder. The high degree of grain refinement in the cryomilled powder was qualitatively indicated by peak broadening observed in the corresponding XRD spectrum as compared to that of the as-received conventional powder (Fig. 20.11).

Klug *et al*.[34] and Suryanarayana[35] provide details of how peak broadening is associated with the small grain size structure of the powder and microstrain introduced into the material during processing. Although the XRD spectra provided a good indication that cryomilling of NiCrAlY powder produced fine microstructure, e.g. grain size, TEM analysis more accurately revealed the actual grain size, as well as other micro- or nano-scopic features, e.g. dislocations, stacking faults, etc. (Fig. 20.12, top). The TEM results indicated an average grain size of 26 ± 8 nm within the cryomilled powder.

An important feature in milled powder was the in-situ formation of dispersoids.[36–40] In addition to the presence of phases from the NiCrAlY, the diffraction pattern from the TEM analysis revealed the presence of Al_2O_3 and AlN (Fig. 20.12, bottom). These two phases represented dispersoids that were formed when aluminum present in the alloy reacted with oxygen in the system, e.g. gaseous oxygen, or within the passivated layer of the particles, and nitrogen in liquid form. The iron phase also present in the cryomilled powder was contamination from the stainless steel milling media and chamber wall.

The DJ 2700 (Sulzer Metco) HVOF system was used to deposit coating samples from cryomilled powder (Fig. 20.13). The coating had a fairly low porosity level at less than 1% and an average microhardness of approximately 440 $HV_{0.3}$. The backscattered electron image of the nanostructured NiCrAlY coating

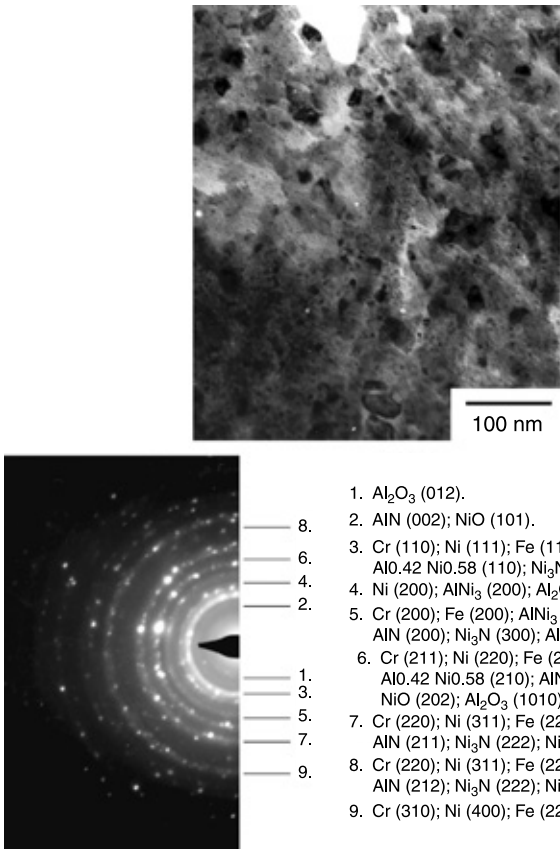

20.12 Transmission electron microscopy micrograph of cryomilled NiCrAlY powder (top) and diffraction pattern and indexing results (bottom).

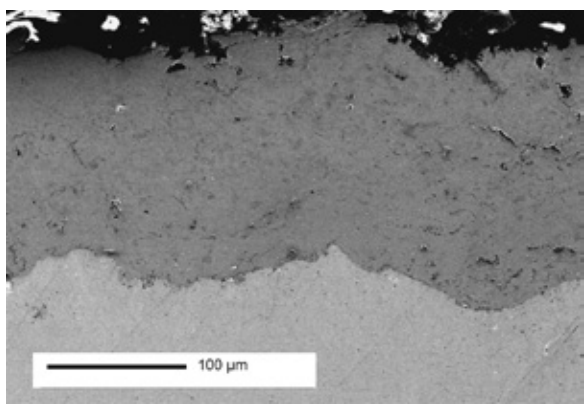

20.13 Cross-section of HVOF-applied nanostructured NiCrAlY coating.

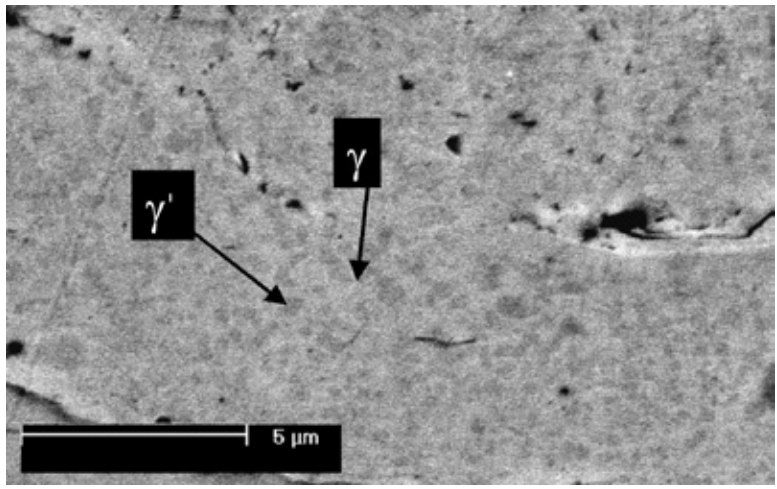

20.14 Backscattered electron image of HVOF applied nanostructured NiCrAlY coating.

showed a structure composed mainly of two phases γ (Ni solid solution) and γ' (Ni_3Al), as in Fig. 20.14. The bright and dark regions correspond to the γ and γ' phases, respectively. Figure 20.15 provides the TEM analyses of the nanostructured coating.

The two notable features were that there were no longer any signs of AlN phase and that the grain size was not uniform. The absence of AlN in the nanostructured coating was likely a result of its decomposition and oxidation during HVOF processing. The grain size distribution in the nanostructured NiCrAlY coating was 'multimodal' in structure, nano-grained regions (approximately 75 nm), ultrafine-grained regions (100–550 nm), and submicron-grained regions (<1 µm).

The static oxidation test at 1000°C yielded notable differences in the type of thermally grown oxide (TGO) that formed on the surfaces of the conventional and nanostructured NiCrAlY-only coating samples. It became apparent that the nanostructured coating quickly formed a continuous, stable, and preferred α-Al_2O_3 TGO layer, which mitigated further oxidation of the coating surface (Fig. 20.16). On the other hand, the conventional coating quickly formed a TGO consisting of non-continuous α-Al_2O_3 layer with protrusions of mixed oxides (Fig. 20.17). It is well accepted within the TBC community that delaying the formation of mixed oxides, which is associated with higher growth rate, is an important factor in extending the life of TBCs.[41,42] After 95 hrs, the formation of mixed oxides was observed on the nanostructured coating samples (Fig. 20.18).

A re-oxidation test was carried out on nanostructured coating samples that had already been exposed to the 1000°C static oxidation test. As a result of having been exposed to high temperatures, these samples' grain size had increased to the

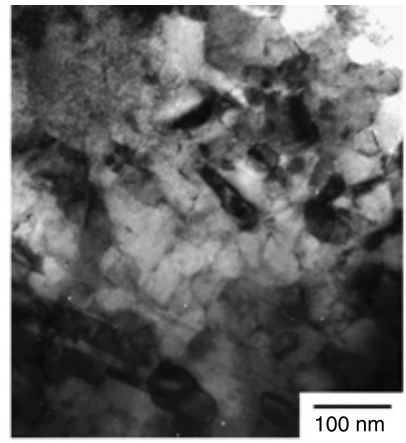

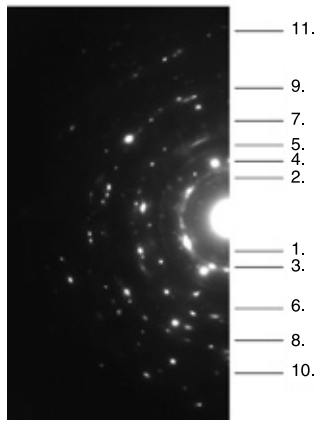

1. Cr (200); NiO (101); Cr_2O_3 (110); Al_2O_3(104); $AlNi_3$ (110).
2. Cr (210); Ni (111); Fe (110); Al0.42 Ni0.58 (110); $AlNi_3$ (111); Al_2O_3 (113).
3. Cr (220); Ni (200); $AlNi_3$ (200); Cr_2O_3 (024).
4. Cr (222); Fe (709); Al0.42 Ni0.58 (200); $AlNi_3$ (211); NiO (104); Cr_2O_3 (214); Al_2O_3 (122).
5. Cr (400); Ni (220); Al0.42 Ni0.58 (210); $AlNi_3$ (220); NiO (113); Cr_2O_3 (1010); Al_2O_3 (1010).
6. Cr (421); Ni (311); Al0.42 Ni0.58 (220); $AlNi_3$ (311); NiO (024); Al_2O_3 (128).
7. Cr (521); Ni (400); Fe (310); Al0.42 Ni0.58 (310); $AlNi_3$ (400); NiO (214); Al_2O_3 (1211).
8. Cr (611); Ni (331); Fe (222); $AlNi_3$ (331); Al_2O_3(416).
9. Fe (321).
10. Fe (330).
11. Fe (332).

20.15 Transmission electron microscopy micrograph of nanostructured NiCrAlY coating (top) and diffraction pattern and indexing results (bottom).

range of as-sprayed conventional coatings. The objective of this test was to determine whether or not the preference for the nanostructured coating to form a α-Al_2O_3 TGO layer was linked to the bond coat's fine grain structure. Interestingly, the static re-oxidation test results showed similar affinity for the formation of α-Al_2O_3 TGO layer (Fig. 20.19). The isolated regions where mixed oxide protrusions were visible corresponded to areas where the aluminum content was depleted prior to carrying out the re-oxidation test. These results indicated that the origins for preferential α-Al_2O_3 TGO layer formation were not, at least solely, a result of fine grain structure. Current hypothesis is that the preference in nanostructured NiCrAlY coatings towards the formation of an α-Al_2O_3 TGO layer is linked to the presence of the previously mentioned alumina dispersoids

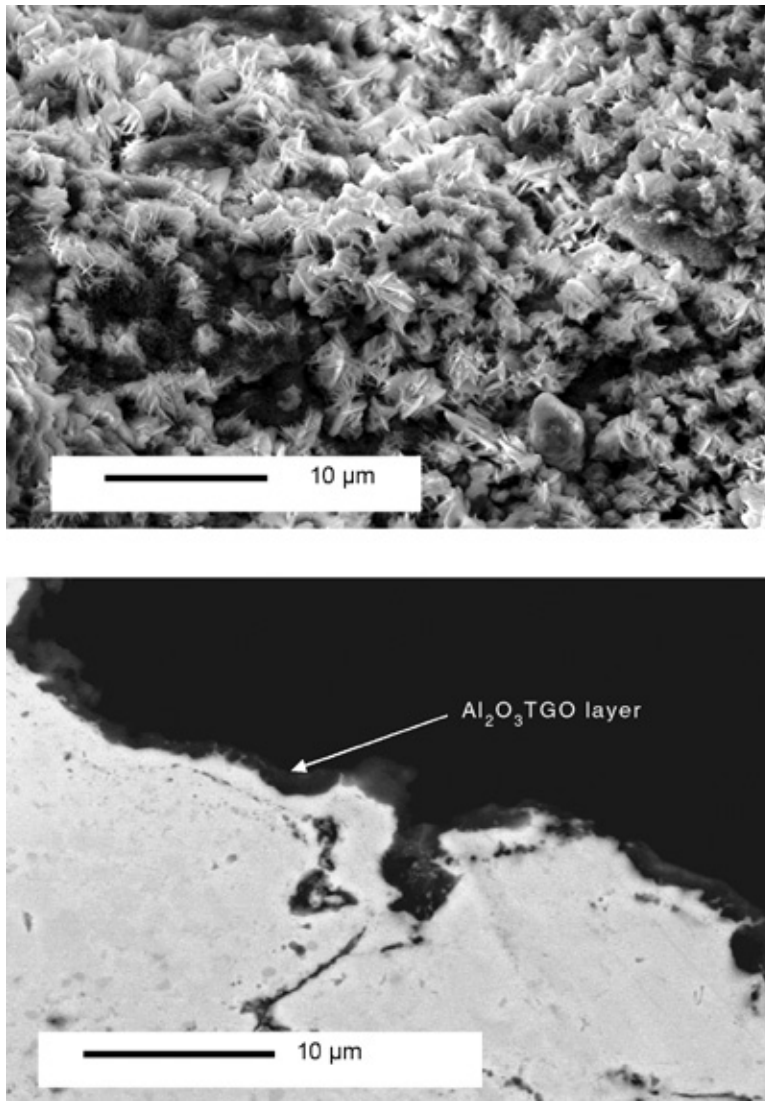

20.16 TGO formation on nanostructured NiCrAlY coating – top (top) and cross-sectional (bottom) views.

that are formed during cryomilling and retained in the coating after spraying (Fig. 20.20). Wu *et al*.[43] have observed the same response when an Al_2O_3 second phase was incorporated into NiCrAlY coatings obtained by plasma-laser technique. It seems that the Al_2O_3 dispersoids act as nucleation sites and/or hinder the diffusion of Ni and Cr to the coating surface when exposed to high temperatures.

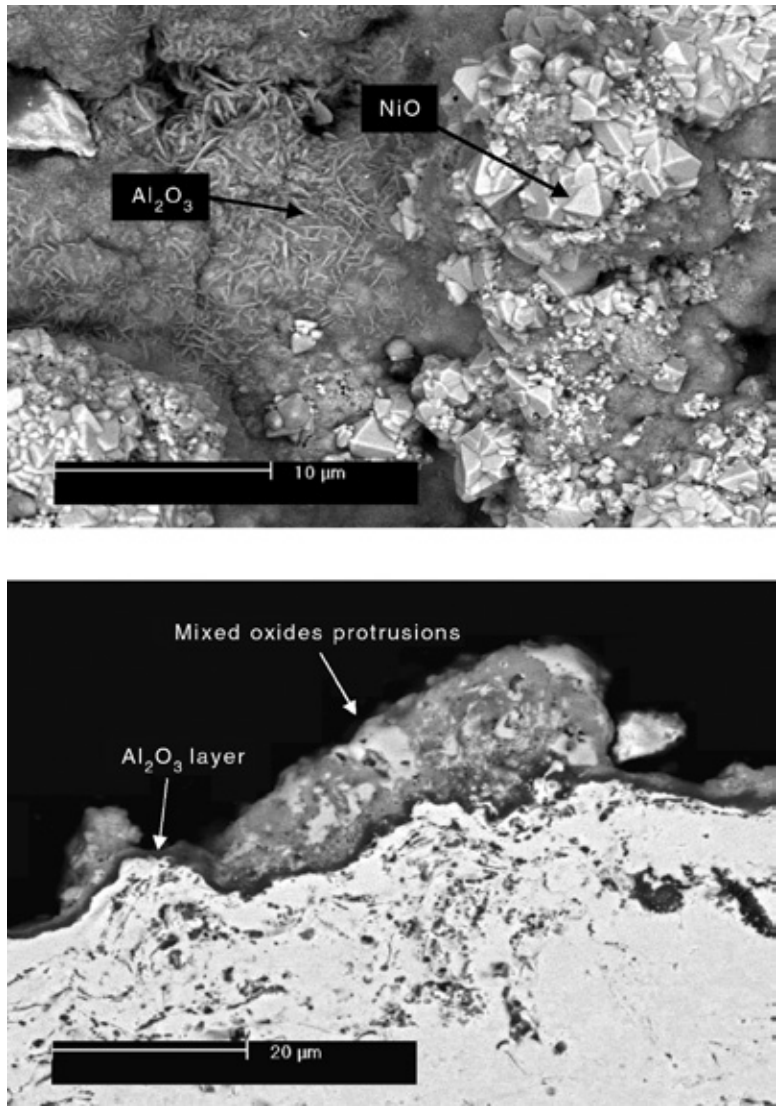

20.17 TGO formation on conventional NiCrAlY coating – top (top) and cross-sectional (bottom) views.

To compare thermal cycling performances between TBC samples with nanostructured and conventional bond coats, 25 mm diameter by 3 mm thick Hastelloy X substrates were prepared. Each sample consisted of an HVOF or LPPS sprayed (100–150 μm thick) NiCrAlY bond coat with an APS sprayed (250–300 μm thick) YPSZ top coat. The TBC samples were then heat treated in

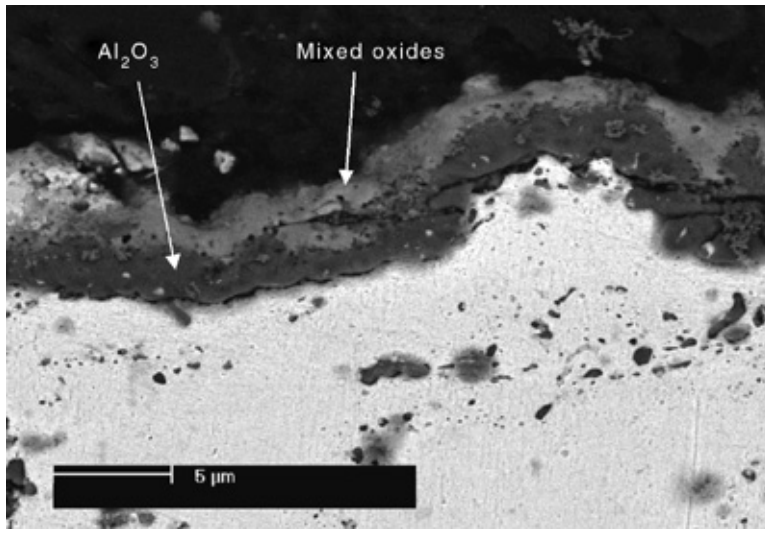

20.18 TGO formation on nanostructured NiCrAlY after 95 hrs at 1000°C.

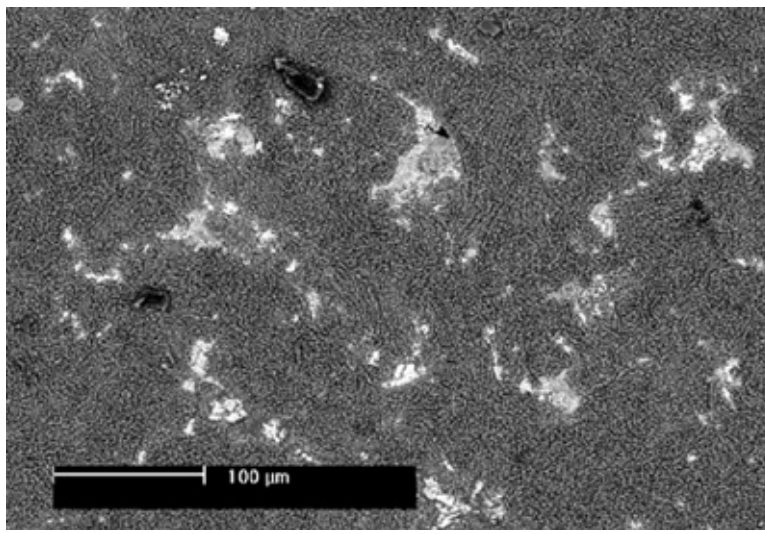

20.19 Top view of TGO formation on re-oxidized nanostructured NiCrAlY coating.

vacuum at 1080°C for four hours prior to undergoing the thermal cycling test. The TBC samples with nanostructured bond coat outperformed those with conventional bond coat by more than 50%, with TBCs with LPPS nanostructured bond coat leading the way (Fig. 20.21). The majority of the TBC samples showed the

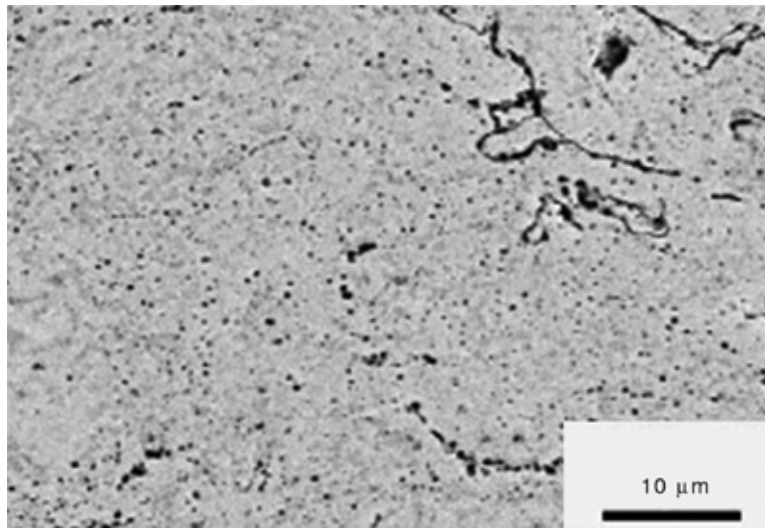

20.20 Dispersoids in nanostructured NiCrAlY coating.

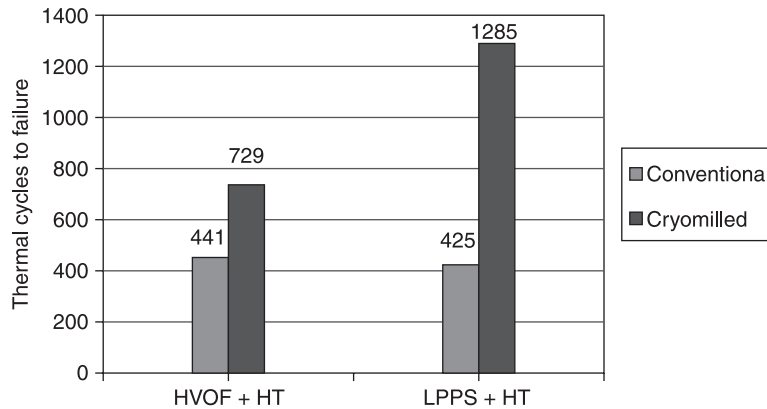

20.21 Thermal cycling results for TBC samples with conventional and nanostructured NiCrAlY bond coats.

presence of mainly α-Al_2O_3 TGO with a small amount of discrete yttrium aluminum oxide particles. There was an obvious difference in TGO growth rate for TBC samples with LPPS applied conventional and nanostructured NiCrAlY, with the latter showing a notably slower rate and longer cycles to failure (Fig. 20.22).[44] There was no obvious link between TGO growth rate and number of cycles to failure for TBC samples with HVOF bond coats; hence, there may be other mechanism(s) affecting these TBC samples' performance.

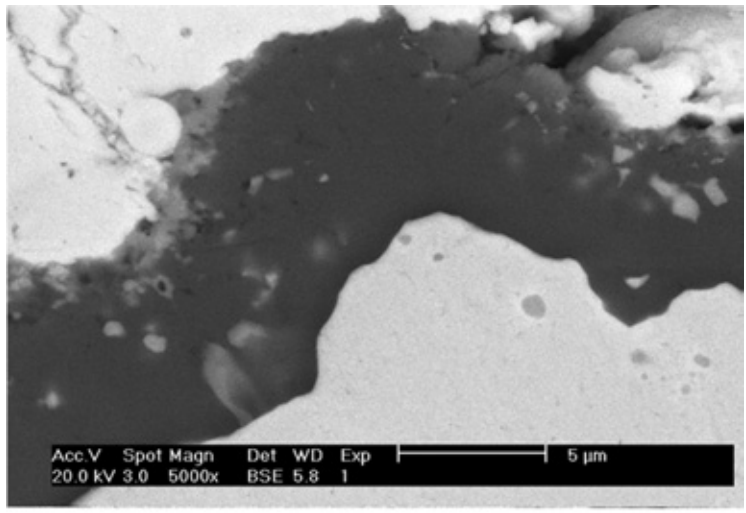

LPPS B 425 cycles

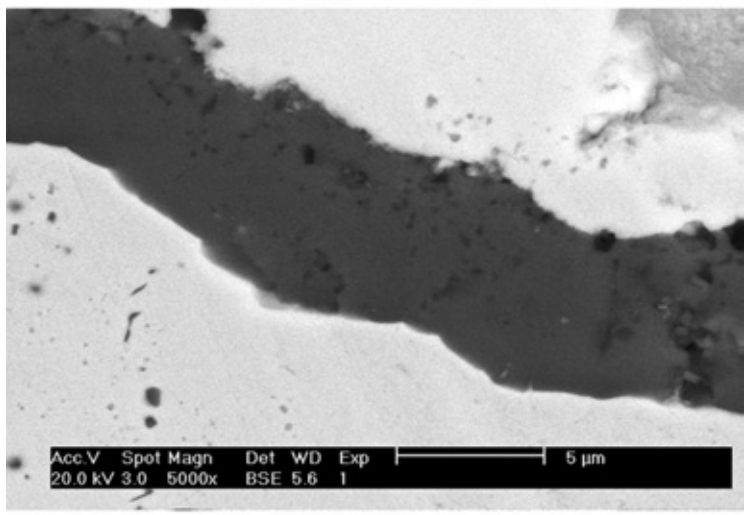

LPPS D 1285 cycles

20.22 TGO of failed TBC samples with conventional (top) and nanostructured (bottom) bond coats following thermal cycle testing.

The presence of the fine- or nano-dispersoids may enhance the life of TBCs by one or more of the following mechanisms:

- enhanced alumina formation and lower TGO growth rate;
- a better coefficient of thermal expansion (CTE) match between top and bond coats;
- increased bond coat creep resistance;
- slower diffusion of Ni and Cr to the coating surface; and
- reduced interdiffusion between bond coat and substrate.

Anyone who has studied TBCs knows how complex the system is with regards to failure mechanisms and life prediction. The experience gained with nanostructured NiCrAlY bond coats shows promising results; however, there needs to be much greater detailed evaluation to understand and further optimize the mechanisms that exist in this new approach.

20.7.2 Manufacturing MCrAlY and NiCrAlY coatings by non-cryogenic milling (n-WERKZ powder)

Since its inception in 2003, n-WERKZ Inc has developed a non-cryogenic milling (NCM) means of processing nanostructured metal powders, including NiCrAlY. Based on the availability of this new commercially viable powder, a new effort to deposit and evaluate the n-WERKZ NiCrAlY powders for TBC applications was initiated in 2007. The goal was to determine whether or not an n-WERKZ nanostructured NiCrAlY powders would be able to form coatings with enhanced oxidation and thermal cycling characteristics, similar to those of cryomilled powder. NiCrAlY with and without top coats were deposited using HVOF. All the top coats were applied via APS. Characterization of n-WERKZ powders and coatings as well as thermal tests on coating samples was carried out.

The n-WERKZ NiCrAlY powder had an average particle size of 34 μm as compared to the as-received average particle size of 21 μm. Figure 20.23 provides a magnified view of the n-WERKZ powders. As expected, there is a strong resemblance in powder morphology when compared to the same powder that has undergone the cryomilling process. The XRD analyses (Fig. 20.24) results show refinement in the grain structure of the n-WERKZ powder.

The Jet Kote HVOF system from Deloro Stellite was used to deposit coating samples from n-WERKZ and conventional powders (Fig. 20.25). The spray parameters corresponded to coating quality qualified by a major gas turbine engine original equipment manufacturer (OEM) for this material; no optimization of the spray parameters was made for the n-WERKZ powder. The coatings had fairly low porosity levels at less than 1% and an average microhardness of approximately of 515 and 522 $HV_{0.3}$ for the conventional and n-WERKZ coatings, respectively.

The static oxidation test at 1000°C yielded comparative results, similar to the conventional and cryomilled NiCrAlY samples, between the TGO formed on the

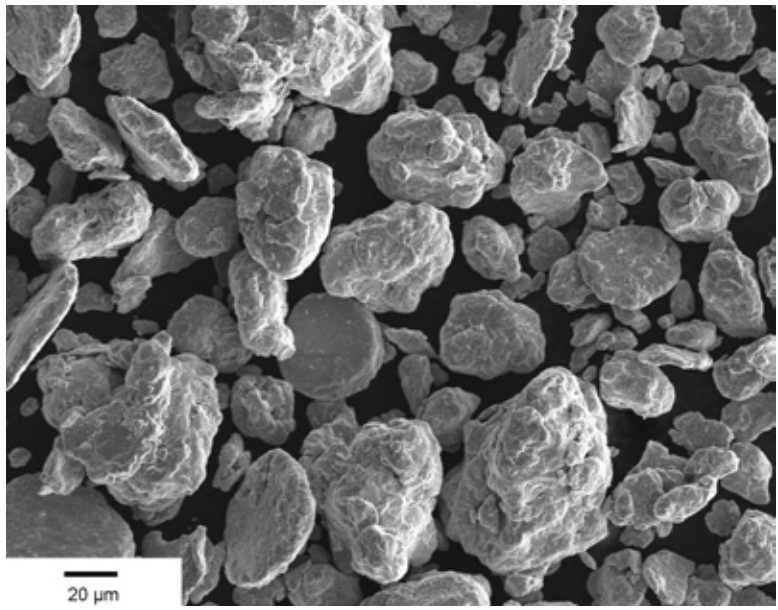

20.23 Non-cryogenically milled (NCM) NiCrAlY powder.

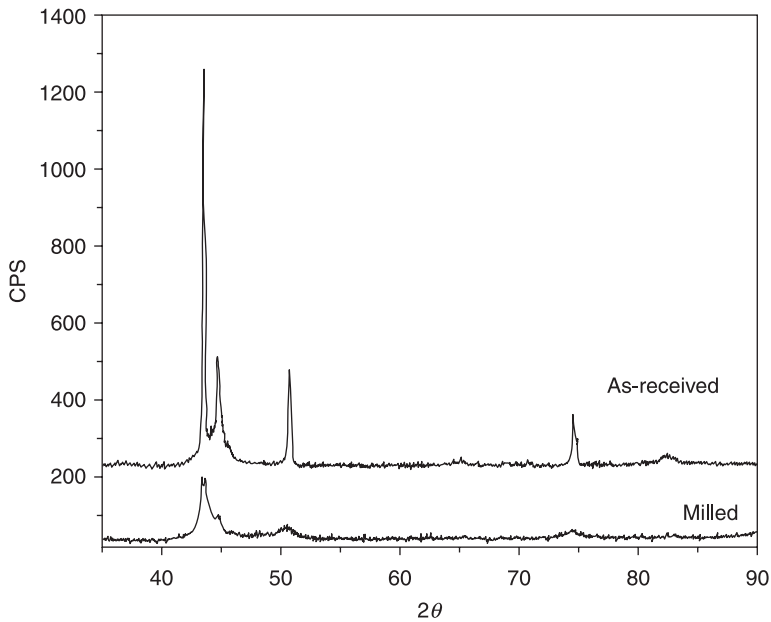

20.24 X-ray diffraction spectra for the as-received and NCM NiCrAlY powders.

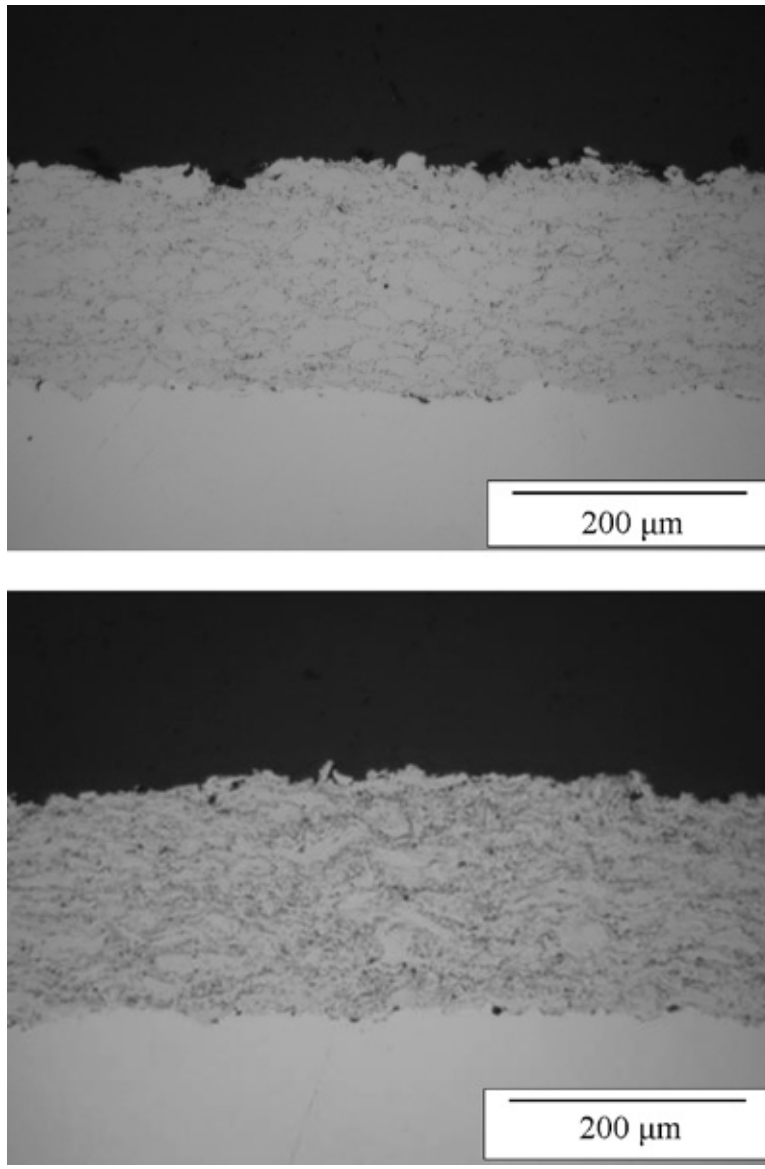

20.25 Cross-sectional view of HVOF-applied conventional (top) and NCM nanostructured (bottom) NiCrAlY coatings.

surfaces of the conventional and n-WERKZ NiCrAlY-only coating samples. A continuous, stable, and preferred α-Al_2O_3 TGO layer formed on the surface of the n-WERKZ coating after 95 hrs of exposure time (Fig. 20.26, bottom); whereas the conventional coating formed a TGO consisting of a non-continuous α-Al_2O_3

layer with protrusions of mixed oxides (Fig. 20.26, top). It is noteworthy that even after 95 hrs, the n-WERKZ coating did not form mixed oxides, as compared to the cryomilled coating, which eventually formed a mixed oxide TGO after exposure to the same conditions and time.

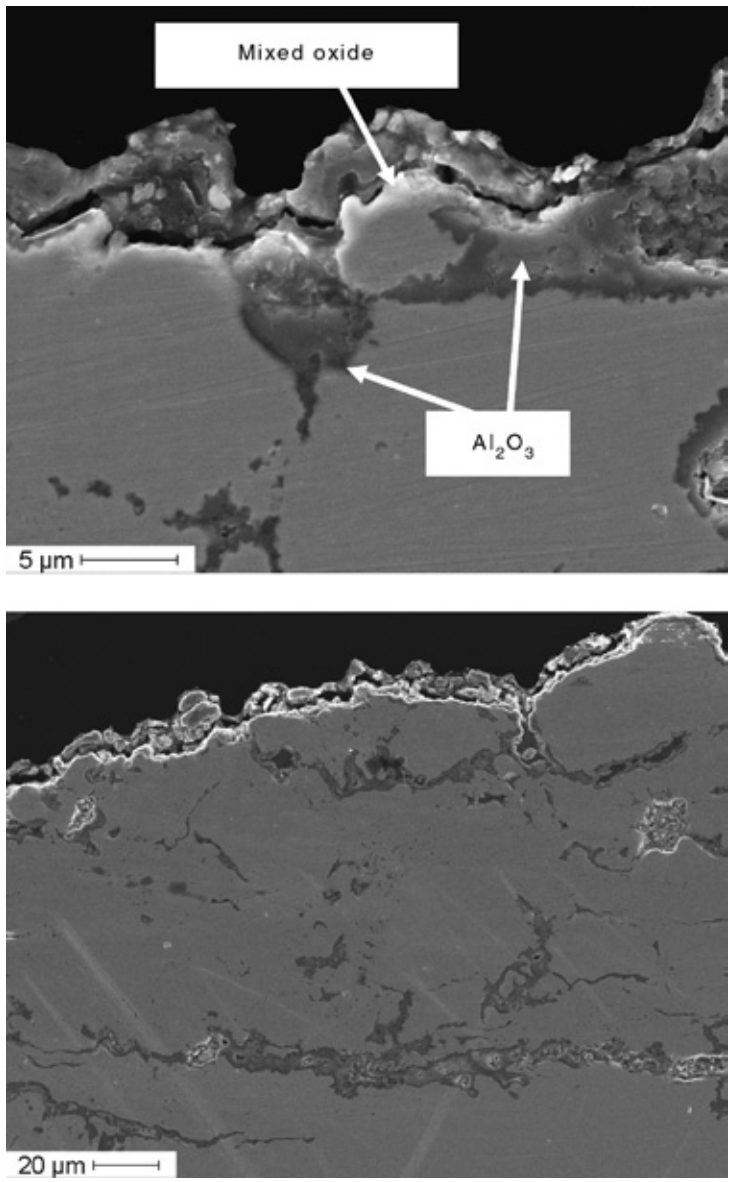

20.26 Cross-sectional view of HVOF-applied conventional (top) and NCM nanostructured NiCrAlY coating after 95 hrs heat treatment (bottom).

TBC samples with n-WERKZ and conventional bond coats were processed onto 25 mm diameter by 3 mm thick Hastelloy X substrates. Each sample consisted of a Jet Kote sprayed (100–150 μm thick) NiCrAlY bond coat with an APS sprayed (250–300 μm thick) YPSZ top coat. The TBC samples were tested as-sprayed, without post-spray heat treatment. The average of three TBC samples with n-WERKZ bond coat outperformed the best performing conventional bond coat by approximately 50% (Fig. 20.27).

Failure analyses of the thermal cycle samples were carried out at the US Naval Academy. As often observed in thermal sprayed TBCs, failure occurred mostly within the YPSZ top coat layer adjacent to the TGO layer (Fig. 20.28).

The notable differences between failed TBC samples with n-WERKZ bond coat and those with conventional bond coat consisted of the following:

- n-WERKZ NiCrAlY had thicker and more continuous α- Al_2O_3 TGO layer, and very few and isolated regions consisting of mixed oxide;
- conventional NiCrAlY had duo layers consisting of Al_2O_3 and mixed oxide TGO layers with an overall thickness that seemed lower (note that these samples failed at least 30% sooner) upon failure.

At the present time, it is believed that the presence of the fine- or nano-dispersoids, i.e. Al_2O_3, formed during the n-WERKZ process, was the source of the enhanced thermal properties of the n-WERKZ nanostructured NiCrAlY coating. The presence of the dispersoids may positively influence the thermal performance of the nanostructured coatings by accelerating the formation of a protective α-Al_2O_3 TGO that will mitigate the further oxidation of the NiCrAlY coating. This in turn may decrease the coefficient of thermal expansion (CTE) of the bond coat to

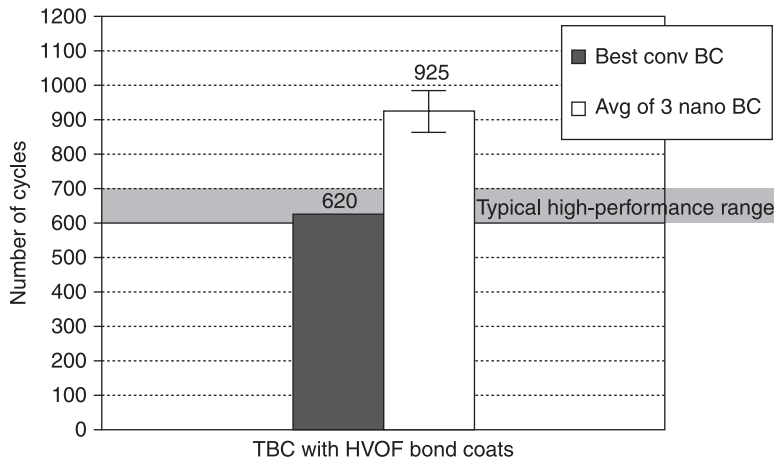

20.27 Thermal cycling test results for TBCs with conventional and NCM nanostructured NiCrAlY bond coats.

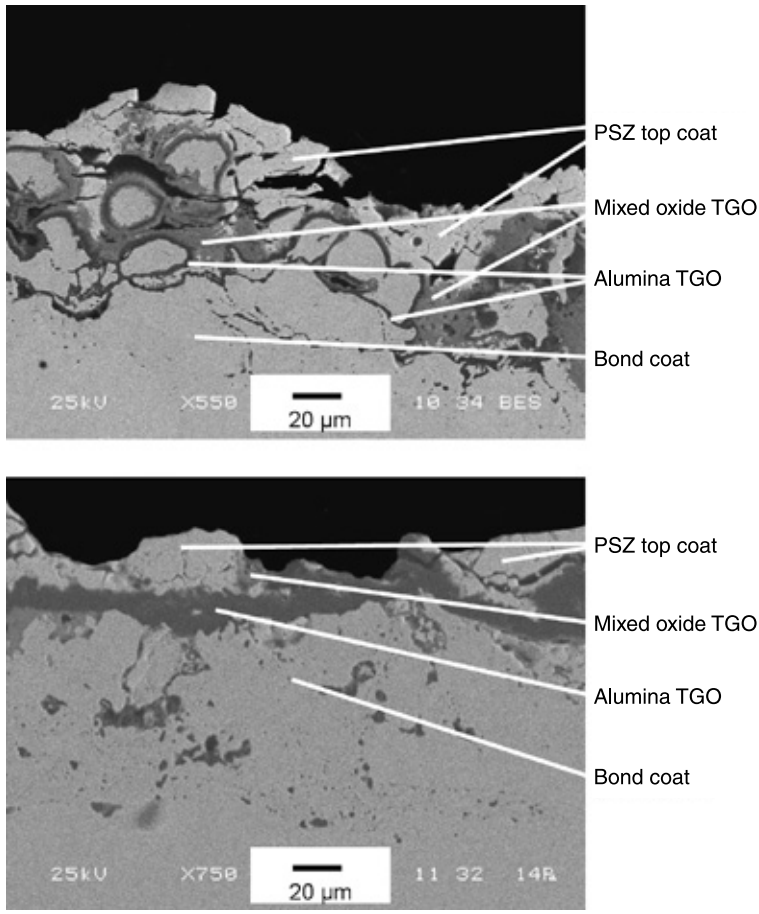

20.28 TGO of failed TBC samples with conventional (top) and NCM nanostructured (bottom) bond coats following thermal cycle testing.

reduce its mismatch with the YPSZ top coat in a TBC system, increasing bond coat creep resistance, and slowing down interdiffusion between bond coat and substrate. As noted in the previous section, more detailed study of these new coatings is required to better understand the mechanisms associated with nanostructured MCrAlYs.

Professor Brochu and his group at McGill University have carried out parallel efforts in the processing and testing of nanostructured NiCoCrAlY for petrochemical applications.[45,46] The results from their study support the findings presented in this chapter. Table 20.1 shows the type of TGO growth observed on nanostructured and conventional-microstructured CoNiCrAlY powders. As observed in NiCrAlY coatings, the cryomilled nanostructured CoNiCrAlY

Table 20.1 Oxide scale at different temperature as a function of the starting grain size

	Starting grain size	
	30–40 nm	3–4 μm
500°C	α-Al_2O_3	Cr_2O_3
800°C	α-Al_2O_3	Cr_2O_3 Al_2O_3•Cr_2O_3
1000°C	α-Al_2O_3	Cr_2O_3 Al_2O_3•Cr_2O_3

powder formed the favorable α-alumina TGO, as opposed to chromia and mixed oxide TGO formed on the conventional CoNiCrAlY powder. This data shows similar attributes between the coatings sprayed using non-cryogenically milled powder and their cryomilled counterpart. The advantages of the NCM process are lower cost, shorter processing time, and easier scalability.

20.8 The cold spray process

Cold spray is a materials deposition process whereby combinations of metallic and non-metallic particles are consolidated to form a coating or freestanding structure by means of ballistic impingement upon a suitable substrate.[47,48,49] The particles utilized are in the form of commercially available powders, typically ranging in size from 5 to 100 μm, which are accelerated from 300 to 1500 m/s by injection into a high-velocity stream of gas. The high-velocity gas stream is generated via the expansion of a pressurized, preheated, gas through a converging–diverging de Laval rocket nozzle. The pressurized gas is expanded to supersonic velocity, with an accompanying decrease in pressure and temperature.[50,51,52] The particles, initially carried by a separate gas stream, are injected into the nozzle either prior to the throat of the nozzle or downstream of the throat. The particles are subsequently accelerated by the main nozzle gas flow and are impacted onto a substrate after exiting the nozzle (Fig. 20.29). Upon impact, the solid particles deform and create a bond with the substrate.[53,54] As the process continues, particles continue to impact the substrate and form bonds with the consolidated material resulting in a uniform deposit with very little porosity and high bond strength. The term 'cold spray' has been used to describe this process due to the relatively low temperatures (–250 to –100°C) of the expanded gas stream that exits the nozzle. This is illustrated in Fig 20.30, which uses a cold spray model developed by Helfritch *et al*.[55] to calculate the temperature of the gas as it expands from the nozzle as a function of inlet temperature and pressure.

The temperature of the gas stream is always below the melting point of the particulate material during cold spray, and the resultant consolidated material is

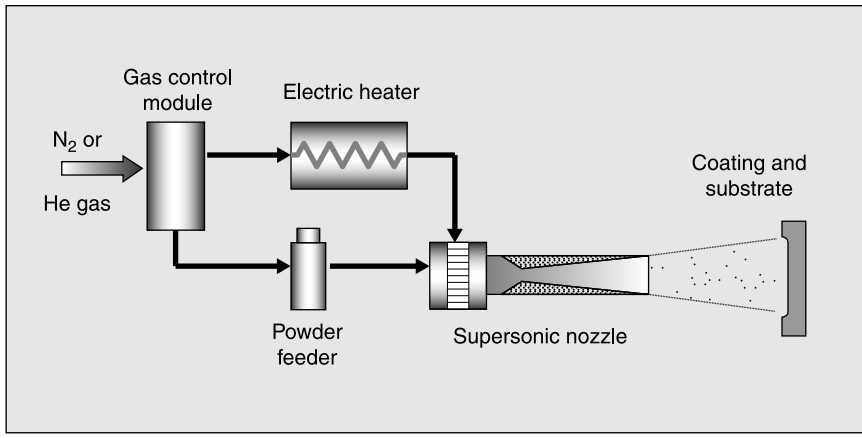

20.29 Schematic of cold spray system.

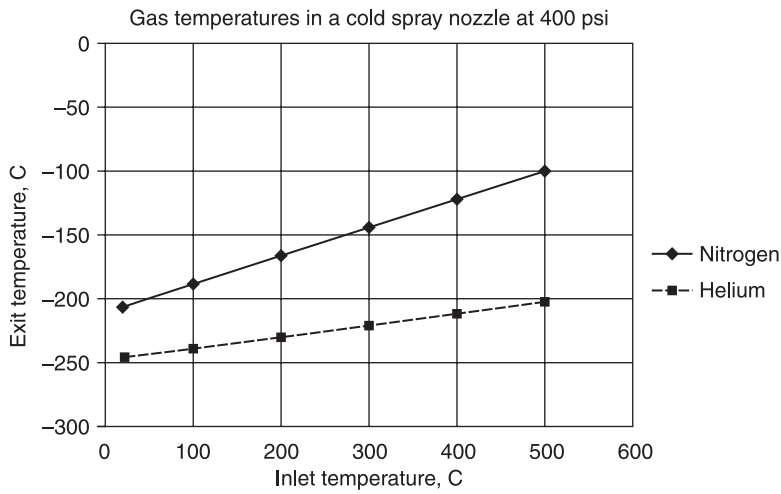

20.30 Gas exit temperature calculated with nitrogen and helium gas as a function of temperature of 400°C and with a main gas pressure of 400 psi using a cold spray nozzle.

formed in the solid state. Since the adhesion of the powder to the substrate, as well as the cohesion of the deposited material, is accomplished in the solid state at low temperatures, the characteristics of the cold spray material are quite unique in many regards. The low temperatures associated with the cold spray process are desirable when nanostructured powders are used as feedstock because the risk of grain growth and phase transformation is minimal or nonexistent. In addition, particle oxidation is avoided, as well as deleterious tensile stresses that occur

during thermal contraction. Therefore, cold spray has the potential to produce nanostructured coatings with a bond strength superior to that of the substrate. With further advancement of techniques to manufacture "cold spray" powders, greater cohesive strength should be possible when compared to conventional thermal spray and powder metallurgy processes.

Cold spray is often compared to traditional thermal spray processes. Although there are certain similarities, it is important to recognize the fundamental differences between the two approaches in order to determine which technique is best suited for the development of nanostructured materials.

Cold spray technology is the logical choice for applications where the high temperatures associated with conventional thermal spray technology can result in undesirable metallurgical transformations, including grain growth, as well as oxidation that can have detrimental effects on bond strength and porosity. Cold spray incorporates very high particle velocities (300–1500 m/s) to achieve consolidation, and gas temperatures can be adjusted to avoid undesirable transformations in the feedstock, the resultant deposit, and the substrate, yielding a deposit with low porosity, high bond strength and increased cohesive strength.

One of the most deleterious effects of depositing materials at high temperatures is the tensile residual stress that develops, especially at the substrate-coating interface, which is the result of the thermal contraction of the molten particles upon solidification. This can become a particular concern in an application where a layer of nanostructured material is to be deposited onto the surface of another material. These stresses often cause delamination, and limit the maximum deposit thickness that can be achieved. This problem is compounded when the substrate material is different from the coating material in terms of hardness and density and there is a significant variation in the coefficient of thermal expansion.

In contrast, there is very little thermally induced dimensional change of the cold spray material since consolidation of the particles takes place in the solid state. Also, the significantly high impact velocities of the solid particulates are very effective at peening the underlying material and producing deposits that are typically in a state of compressive stress.[56] In addition, interfacial instability due to differing viscosities, along with the resulting interfacial roll-ups and vortices, promote interfacial bonding by increasing the interfacial area, giving rise to material mixing at the interface and providing mechanical interlocking between the two materials.[57] Adhesion of thermal spray coatings relies primarily upon the surface finish referred to as the anchor tooth profile of the substrate. The molten particles or 'splats', which are propelled onto the substrate penetrate and subsequently solidify, locking themselves mechanically within the valleys of the surface profile. Except for some of the HVOF coatings that contain carbides or extremely hard particles, there is a significant difference between the bonding mechanism of thermal spray and cold spray.

In comparison with conventional thermal spray techniques, the materials produced by cold spray are typically less porous, with higher hardness and

conductivity and lower oxide concentration. The Young's moduli of cold-sprayed deposits have been reported to be greater than 80% of bulk values.[58] The Army Research Lab (ARL) has developed a cold spray process for depositing 6061 aluminum that has achieved an ultimate tensile strength, yield point and Young's modulus greater than what has been reported in literature for wrought 6061-T6, which is solutionized, quenched and tempered, while the properties of the cold spray coating were taken in the as-sprayed condition. These characteristics are achieved because cold particles are less susceptible to oxidation, and a high velocity impact creates dense, well-consolidated material. The superior qualities of cold-sprayed materials are required by certain applications. For example, the high heat transfer coefficient and electrical conductivity of cold spray materials favor their use in electronic applications.[59] Good corrosion protection is also achieved by dense, impermeable, cold-sprayed coatings.

20.9 Characteristics of cold spray material

Nanostructured materials as defined within the context of this section are those materials whose grain size has dimensions in the 1 to 100 nm range.[60] Osmotic consolidation, pressure filtration, and tape casting have been used to produce consolidated nanostructured materials with limited thickness. Cold spray has been investigated to produce nanostructured coatings, as well as nanostructured bulk materials. The typical particle size of stock powders used for cold spray ranges between 5 and 100 μm. Particles that are <5 μm do not have enough momentum to leave the gas stream and impact on the substrate and are simply swept away as the gas flows over the substrate. Hence, nanoparticles cannot be deposited using cold spray. Instead agglomerated nanoparticles or nanostructured powder within the feasible size range is used.

The deposition thickness produced by a single pass of the cold spray nozzle can vary from 0.01 to 1.0 mm, depending on the powder feed rate, nozzle traverse speed, and deposition efficiency. Multiple coating layers can result in deposits several centimeters thick and some materials appear to have no limitation in the thickness that can be achieved. The width of a single pass of a conventional nozzle is approximately 5 mm, and large surfaces can be coated through multiple, slightly overlapping, parallel sweeps. Nitrogen can be used as the accelerating gas to produce a fully dense copper deposit, with several passes resulting in a coating that was approximately 2 mm thick. The individual copper particles consolidate into a dense, uniform deposit, which adheres tightly to the aluminum substrate. The copper is actually mechanically mixed with the aluminum at the interface. The microstructure resulting from the interaction of impacting particles and the substrate is analogous to materials that have been explosively bonded.

Ceramics can also be considered as a suitable substrate for cold spray, and nitrogen can be used as the accelerating gas to deposit copper powder onto a silicon carbide substrate. Single traces of low oxide copper are deposited forming

a uniform and continuous coating. Ceramics such as alumina, silicon carbide, and aluminum nitride have been successfully coated onto by the cold spray process, as well as some composite and polymeric materials.

20.10 Cold-sprayed processing of WC-Co

Cold spray has been used successfully to deposit cermets such as WC-Co[61,62] and also nanostructured WC-Co.[63] The combination of WC and metallic cobalt as a binder is well suited for sintering and results in a system that has desirable properties. Nanostructured feedstock of WC-Co has been produced by dispersing nano-sized WC particles in a suitable solvent with a cobalt binder precursor and spray dried under a controlled atmosphere to form spheroid particles. WC has high solubility in cobalt at elevated temperatures, and, in combination with the ability of liquid cobalt to wet the WC, superior densification can be achieved during sintering. The binder precursor forms small crystals, coating the nanoparticles, and fills in the gaps interconnecting them, making the resultant agglomerate conducive to the cold spray process, which requires a certain degree of plasticity for adequate consolidation. The cobalt binder serves to contain the WC, and the resultant agglomerate, which is approximately 5–50 μm in diameter (Fig. 20.31), has a good combination of high strength, toughness and hardness. The agglomerates have adequate ductility and deform during the cold spray process upon impact, allowing the buildup of material.

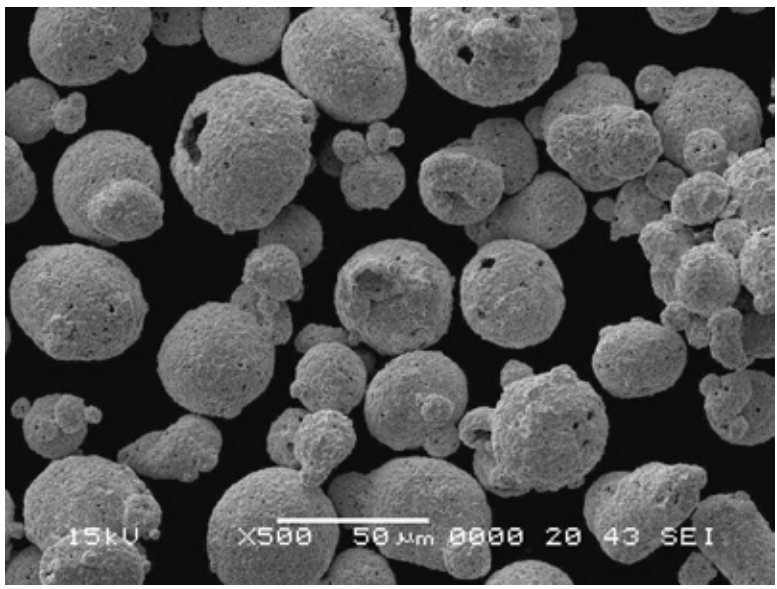

20.31 Agglomerated WC-Co powder.

Figure 20.32 represents an example of the WC-12Co feedstock powder used for cold spray, which consisted of agglomerated submicron particles of WC encapsulated with cobalt. Figure 20.33 shows a cold spray deposit of WC-12Co that was achieved using helium as the accelerating gas. Microstructural characterization of the WC-Co feedstock powder and the resultant cold spray

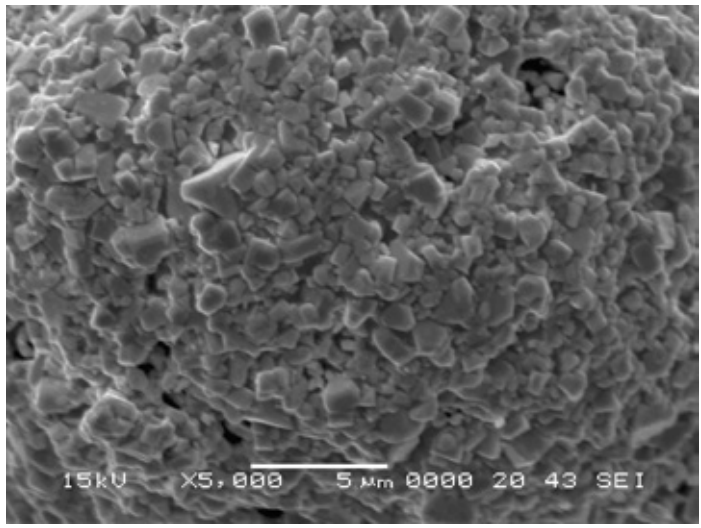

20.32 Submicron particle of WC held together with a cobalt binder.

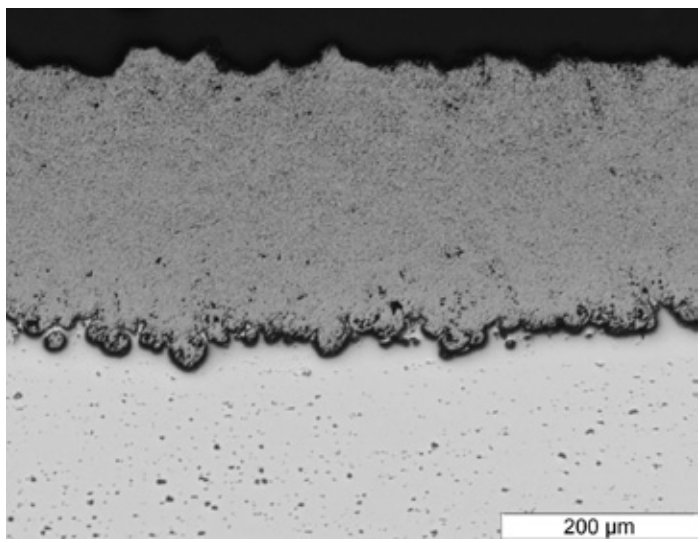

20.33 Cross-sectional view of cold spray WC-Co coating using helium as accelerating gas.

deposits by SEM and X-ray diffraction revealed that there did not appear to be any evidence of phase transformation or decarburization of the WC during cold spray deposition and the original morphology of the submicron particles was unchanged. These are advantages of the cold spray process over thermal spray. Hardness values of 1315 Vickers were also achieved but the resultant coating contained small microcracks. An attempt to mitigate the occurrence of microcracks was undertaken by incorporating nitrogen as the accelerating gas.

Figure 20.34 shows a micrograph of a cross-section of a cold spray deposit using nitrogen. The hardness values were approximately the same, 1300 Vickers, but the overall bond strength of these coatings was lower than those achieved using helium. This was substantiated by the fact that a more aggressive grit blast had to be performed during the surface preparation stage prior to spraying when using nitrogen and the through-thickness hardness values were lower. A 24 grit size alumina had to be used when attempting to cold spray onto hardened (HRC35) 4340 steel, as compared to 60 grit alumina, which was used during the original helium cold spray trials.

The differences in through-thickness hardness was attributed to the fact that nitrogen would result in lower impact velocities, and therefore the particle-to-particle bond would not be as great as that which was achieved using helium, since helium would have much higher impact velocities. In addition, it was determined that there was a greater concentration of WC on the surfaces of those samples produced using nitrogen as the accelerating gas than on those produced using helium because the higher impact velocities associated with helium would also cause an

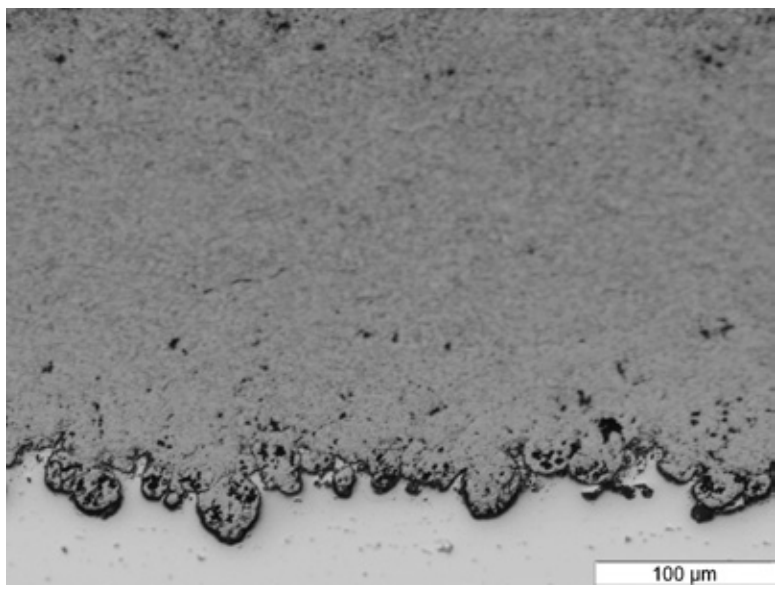

20.34 Interface of cold spray WC-Co coating deposited onto aluminum using nitrogen as accelerating gas.

erosion problem during the cold spray process. This problem could be alleviated by producing feedstock powder that was comprised of WC particles fully encapsulated by a cobalt binder. The feedstock used in this study contained WC particles that were not always adequately coated with cobalt and the exposed areas would erode away the surface of the previous deposit during the cold spray process.

In summary, there has to be more work by powder producers concentrating on the production of 'cold spray' powders to alleviate such problems as erosion during the cold spray process.

20.11 Cold-sprayed processing of non-cryogenically milled n-WERKZ AA5083

The cold spray process was used to consolidate non-cryogenically milled (NCM) AA5083 powder produced by n-WERKZ at the US Army Research Laboratory. The cold spray process operates at temperatures that can exceed 800°C with corresponding pressures greater than 650 psi. Therefore predictive models were used to develop the optimized process parameters that would maintain the nanostructured microstructure. It must be understood that although the cold spray gas temperature may be set well below any critical transformation temperature for AA5083, the kinetic energy of accelerating particles are transferred into thermal energy upon impact. Continuous particle impact events can increase the temperature of the coating/deposit as well as the substrate locally, especially when attempting to build up thick deposits. In addition, aluminum and its alloys also present another challenge with regard to nozzle clogging, which is related primarily to operating temperature. Various nozzle materials have been investigated over the years by ARL and others to mitigate clogging of low temperature materials. A thermally stable amorphous thermoplastic polymer was chosen for this effort.

The predictive models developed by ARL can be used to determine the impact velocity of accelerating particles as well as the 'critical' impact velocity. The critical impact velocity can be defined as that which results in adequate consolidation of the particles. The exact amount of plastic deformation that each particle must undergo to result in an adequate consolidated deposit is still very much under debate, but as Fig. 20.35 indicates, the critical impact velocity is approximately 650 m/s. Incorporating the cold spray process parameters used in this study with the accelerating gas set at a temperature of 400°C and a main gas pressure of 400 psi, a 20 μm particle would achieve an impact velocity of 1438 m/s with helium and 697 m/s in a nitrogen gas stream, (Fig. 20.35). The average particle size for the AA5083 was 56.7 μm, as the data presented in the particle analysis shows (Fig. 20.36). However, this analysis also shows a larger percentage of particles that are >100 μm. The corresponding impact velocity for the average particle size was approximately 850 m/s, as calculated for the accelerating gas set at a temperature of 400°C and a main gas pressure of 400 psi. However, the impact velocity of some of the larger agglomerates (>120 μm) cannot be achieved using

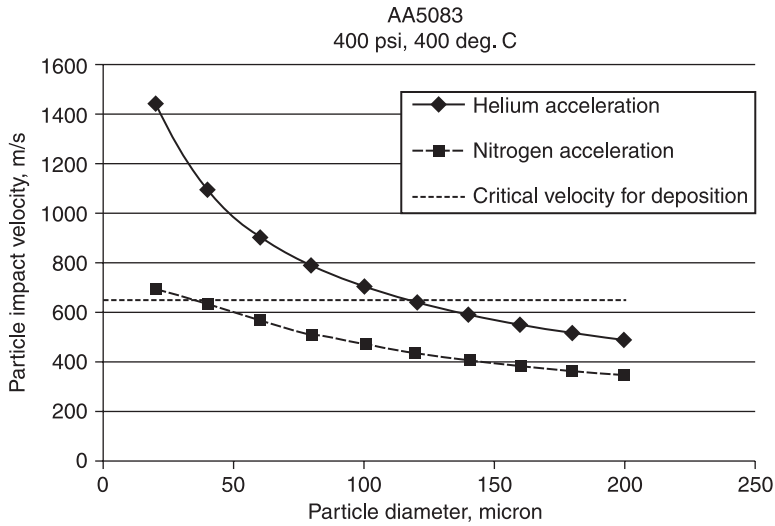

20.35 Critical impact velocity calculated with the helium accelerating gas set at a temperature of 400°C and with a main gas pressure of 400 psi.

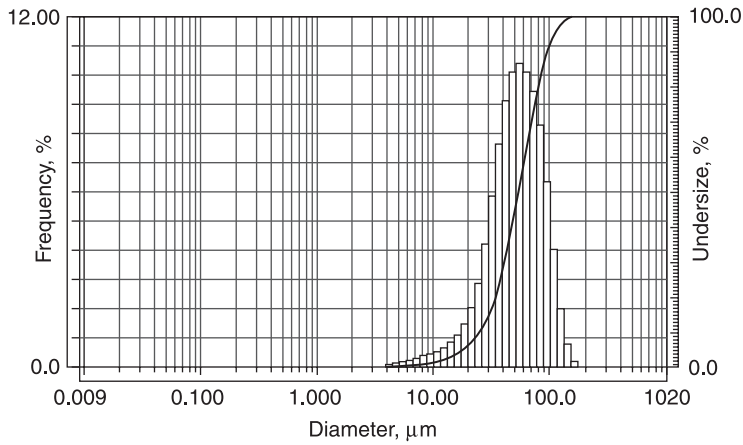

20.36 Particle analysis of the n-WERKZ AA5083 showing the average particle size as approximately 56.7 µm. Note the larger percentage of particles >100 µm.

the process parameters described. This would explain the random voids observed within the structure of the cold spray deposit.

The best operating process parameters were selected based upon several primary factors, including maximum temperature, deposition efficiency, density and nozzle clogging. Helium was used as the accelerating gas at a temperature of approximately 400°C with a pressure of 400 psi. Figure 20.37 shows an as-polished cross-section

of the resultant deposit. Note the 'splat' or particle boundaries and the complete consolidation that was achieved using these process parameters. There were random voids observed within the structure that were later attributed to large agglomerates found in the original feedstock powder (Fig. 20.38). These agglomerates were in excess of 100 μm, and as such would not completely deform during impact, leaving

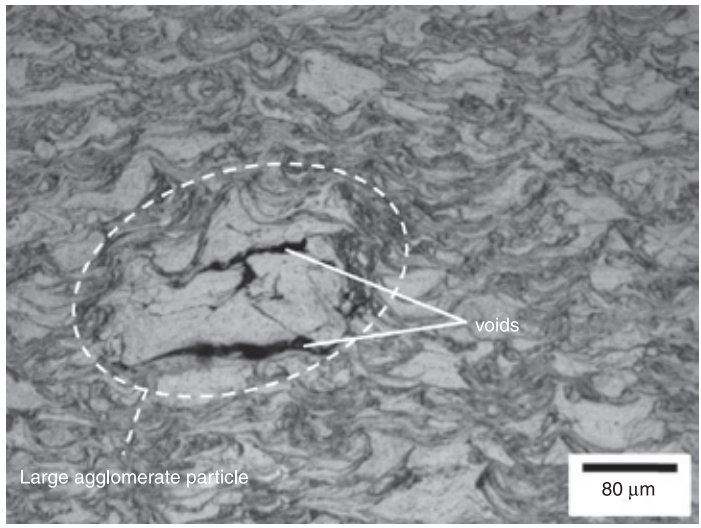

20.37 Optical microscope view of cold spray deposit of n-WERKZ nanostructured AA5083.

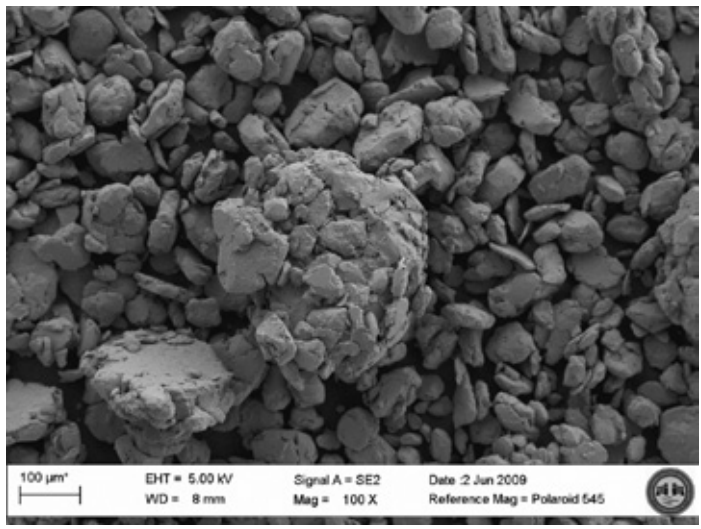

20.38 Original n-WERKZ nanostructured AA5083 feedstock with large agglomerates.

behind these occasional defects. An attempt was made to sieve the feedstock powder using a 325-mesh sieve, which would remove any particle having a diameter greater than approximately 44 μm. The particle size analysis of the sieved powder shows new mean particle size of 33.9 μm, with no particles larger than 65 μm (Fig. 20.39). Additional spray trials were conducted and results indicated the elimination of these voids in the structure of the AA5083 cold spray deposit (Fig. 20.40).

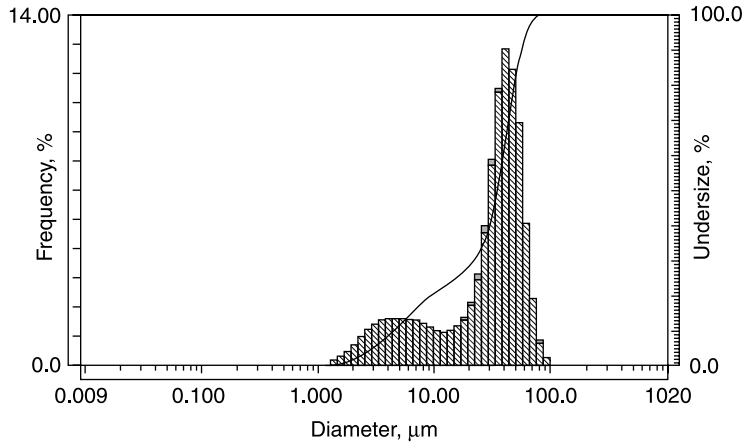

20.39 Particle analysis of the sieved n-WERKZ AA5083 showing the average particle size as approximately 33.9 m.

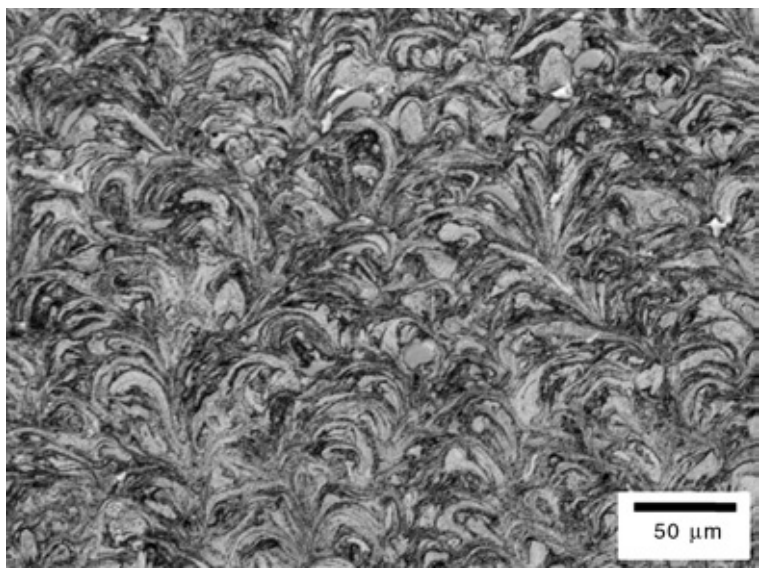

20.40 Optical microscope view of cold spray deposit of sieved n-WERKZ nanostructured AA5083.

A typical bright-field TEM micrograph from cold-sprayed AA5083 is presented in Fig 20.41. Very little porosity and oxide inclusion were observed. Deformation of face-centered cubic (fcc) Al from high particle velocity deposition resulted in elongated grains with aspect ratio ranging from 2~3 to 1. Mean grain size was approximated at 100 ± 35 nm. Between nano-grains, excellent chemical bonding without deleterious voids or inclusions was observed as demonstrated by the high-resolution TEM micrograph in Fig. 20.42. However, inclusions and voids

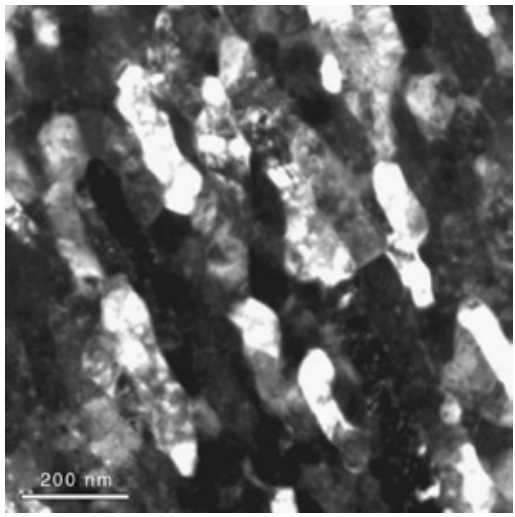

20.41 Bright-field TEM micrograph of cold-sprayed AA5083.

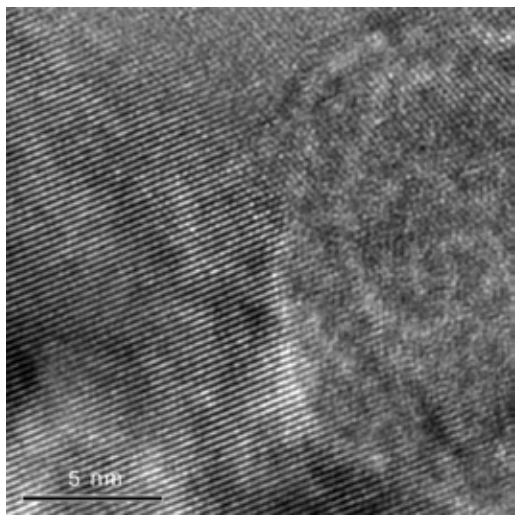

20.42 High-resolution TEM micrograph of grain boundary in cold-sprayed AA5083.

were occasionally observed at splat (e.g. prior particle) boundaries as presented in Fig. 20.43. At the interface between AA5083 cold-sprayed coating and AA6061 substrate, excellent bonding was observed as presented in Fig. 20.44. Certainly, inclusions of oxides were observed but not as a continuous layer since they were

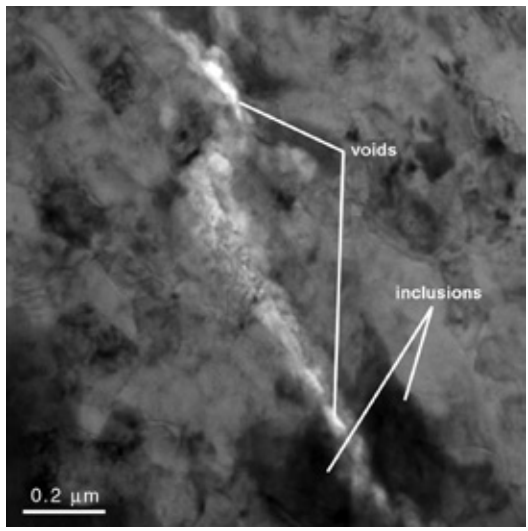

20.43 Bright-field TEM micrograph showing decohesion (white region) and inclusions (dark spots) observed at the splat boundary of cold-sprayed AA5083.

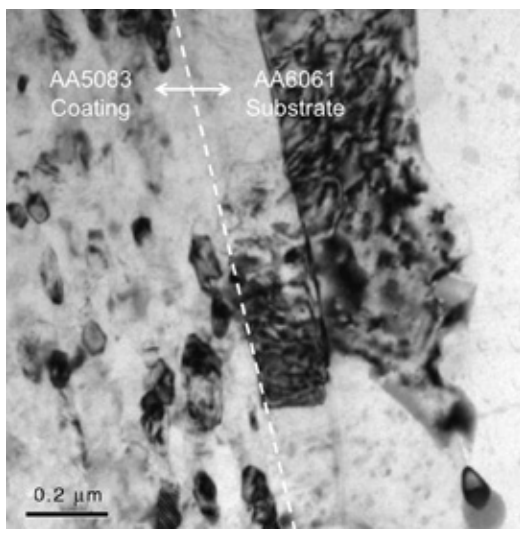

20.44 Bright-field TEM micrograph of coating-substrate interface.

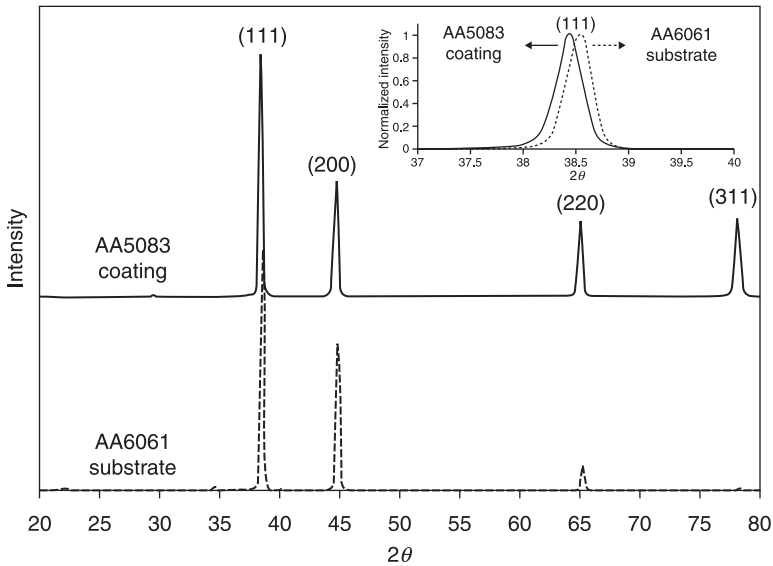

20.45 X-ray diffraction patterns from cold-sprayed AA5083 and uncoated bottom surface of AA6061 substrate.

broken apart due to the deformation of impinging particle associated with high velocity impact. Thus, a majority of the coating/substrate interface consisted of fcc-Al bonding between AA5083 and AA6061. Figure 20.45 presents X-ray diffraction patterns from cold-sprayed AA5083 and annealed AA6061 (e.g. uncoated bottom surface). While both patterns correspond to fcc-Al (i.e. also confirmed by electron diffraction from TEM), a noticeable compressive strain, estimated at 0.31% was observed for the cold-sprayed AA5083 coating.

20.12 Future trends

The low temperature and high kinetic energy associated with the cold spray process allow for the retention of fine/nano-grain structure, absence of phase change, capability for thick deposits, and promotion of compressive residual coating stress. These capabilities make the cold spray process an ideal approach to depositing nanostructured metal-base coatings. In addition to the nanostructured metal-base coatings presented in this chapter, potential nanostructured coating applications may include: MCrAlY coatings for high temperatures; CuCr for oxidation protection; Al and Zn sacrificial cathodic protection coatings; Al- or Cu-base metals or their MMCs for thermal management; Al, Cu, and steel for electronics; Ti and Ta for bioengineering and corrosion protection; and CuNiIn for anti-fretting.

In addition to applications revolving around nanostructured coatings, cold spray of nanostructured metal-base materials may also contribute to stronger near-net-shape spray nanostructured forms, and better repair of worn/damaged components.

20.13 Sources of further information and advice

Additional sources of information pertaining to thermal-sprayed nanostructured metal-base coatings can be found in technical journals relating to thermal spray and/or materials science.

20.14 Acknowledgements

We wish to thank Dr Lawrence T. Kabacoff (ONR), Ken Scandell (NAVSEA), and Linda K. Jensen (Juridica, Inc.) for their constructive contributions towards the preparation and the review of this manuscript.

Special thanks should be given to Jimmy Walker and FW Gartner Thermal Spraying Co. for their contribution of industrial thermal spray processing photographs. As well, we would like to thank Professors Angela L. Moran (US Naval Academy) and Julie Schoenung (UC, Davis), as well as Dr Virgil Provenzano (NIST) for their technical contributions to portions of this chapter.

20.15 References

1 Kabacoff L.T., Nanoceramic Coatings Exhibit Much Higher Toughness and Wear Resistance than Conventional Coatings. The AMPTIAC Newsletter, Spring 2002, Volume 6, Number 1.
2 Shaw L., Luo H., Villegas J., Miracle D. Thermal Stability of Nanostructured Al93Fe3Cr2Ti2 Alloys Prepared via Mechanical Alloying. Acta Materialia 51 (2003), p. 2647.
3 Eigen N., Klassen T., Aust E., Bormann R., Gartner F. Production of Nanocrystalline Cermet Thermal Spray Powders for Wear Resistant Coatings by High-Energy Milling. Materials Science and Engineering A356 (2003) p. 114.
4 Chen Y., Li C.P., Chen H., Chen Y. One-Dimensional Nanomaterials Synthesized using High-Energy Ball Milling and Annealing Process. Science and Technology of Advanced Materials 7 (2006), p. 839.
5 Ye J., Schoenung J.M. Technical Cost Modeling for the Mechanical Milling at Cryogenic Temperature (Cryomilling). Advanced Engineering materials 2004, 6, No. 8, p. 656.
6 Beck R.C.R., Lionzo M.I.Z., Costa T.M.H., Benvenutti E.V., Re M.I., Gallas M.R., Pohlmann A.R., Guterres S.S. Surface Morphology of Spray-Dried Nanoparticle-Coated Microparticles Designed as an Oral Drug Delivery System. Brazilian Journal of Chemical Engineering, 2008, Vol. 25, No. 02, April–June, p. 389.
7 Chaubal M.V., Popescu C. Conversion of Nanosuspensions into Dry Powders by Spray Drying: A Case Study. Pharmaceutical Research 2008, Vol. 25, No. 10, October, p. 2303.

8 Jordan E.H., Gell M. Nano Crystalline Ceramic and Ceramic Coatings Made by Conventional and Solution Plasma Spray. In Nanomaterials Technology for Military Vehicle Structural Applications, Meeting Proceedings RTO-MP-AVT-122, Paper 9. Neuilly-sur-Seine, France, 2005, pp. 9–19.
9 Wang D., Tian Z., Shen L., Liu Z., Huang Y. Preparation and characterization of nanostructured Al_2O_3-13wt.%TiO_2 ceramic coatings by plasma spraying. Rare metals 2009, Vol. 28, no. 5, October, p. 465.
10 Marple B.R., Voyer J., Bisson J.F., Moreau C. Processing and Characterization of Nanostructured Cermet Coatings. Proceedings of the International Thermal Spray Conference (ITSC 2001), Singapore, May 28–30, 2001, p. 343.
11 Bernecki T. Surface Science. In Davis J.R., editor. Handbook of Thermal Spray Technology. ASM International, Materials Park, OH, USA, 2004, p. 14.
12 F.W. Gartner Thermal Spraying Co.
13 Qiao Y., Liu Y.R., Fischer T.E. Sliding and Abrasive Wear Resistance of Thermal-Sprayed WC-Co Coatings. Journal of Thermal Spray Technology, Vol. 10(1), March 2001, p. 118.
14 Guilemany J.M., Dosta S., Miguel J.R. Study of the Properties of WC-Co Nanostructured Coatings Sprayed by High-Velocity Oxyfuel. Journal of Thermal Spray Technology, Vol. 14(3), September 2005, p. 405.
15 He J., Ice M., Dallek S., Lavernia E.J. Synthesis of Nanostructured WC-12 Pct Co Coating Using Mechanical Milling and High-Velocity Oxygen Fuel Thermal Spraying. Metallurgical and Materials Transactions A, Vol. 31A, February 2000, p. 541.
16 Ibrahim A., Berndt C.C. Fatigue and Mechanical Properties of Nanostructured WC-Co Coatings. Proceedings of the International Thermal Spray Conference, May 10–12, 2004, Osaka, Japan, p. 878.
17 Morks M.F., Shoeib M.A., Ibrahim A. Comparative Study of Nanostructured and Conventional WC-Co Coatings. Proceedings of the International Thermal Spray Conference, May 10–12, 2004, Osaka, Japan, p. 857.
18 Zha B., Wang H., Su X., Nano Structured WC-12Co Coatings Sprayed by HVO/AF, Proceedings of the International Thermal Spray Conference, May 10–12, 2004, Osaka, Japan, pp. 881–881.
19 Liu S., Sun D., Fan Z., Yu H.Y., Meng H.M. The influence of HVAF powder feedstock characteristics on the sliding wear behaviour of WC-NiCr coatings. Surface & Coatings Technology 202 (2008), p. 4893.
20 Kim H.J., Lee C.H., Hwang S.Y. Superhard nano WC-12%Co coating by cold spray deposition. Materials Science and Engineering A 391 (2005), p. 243.
21 Smirnov N.I., Prozhega M.V., Smirnov N.N. Study of Tribological Properties of Detonation Nanostructured WC-Co-Based Coatings. Journal of Friction and Wear 2007, Vol. 28, No. 2, p. 200.
22 Zhu Y.C., Yukimura K., Ding C.X., Zhang P.Y. Tribological properties of nanostructured and conventional WC-Co coatings deposited by plasma spraying. Thin Solid Films 388 (2001), p. 277.
23 Jordan E.H., Gell M., Sohn Y.H., Goberman D., Shaw L., Jiang S., Wang M., Xiao T.D., Wang Y., Strutt P. Fabrication and Evaluation of Plasma Sprayed Nanostructured Alumina-Titania Coatings with Superior Properties, Mater Sci Eng, A301, 2001, p. 80.
24 Gell M., Jordan E.H., Sohn Y.H., Goberman D., Shaw L., Xiao T.D. Development and Implementation of Plasma Sprayed Nanostructured Ceramic Coatings, Surface and Coatings Technology,' vol. 146–147, 2001, p. 48.

25 Goberman D., Sohn Y.H., Shaw L., Jordan E.H., Gell M. Microstructure Development of Al2O3-13 wt%TiO2 Plasma Sprayed Coatings Derived from Nanocrystalline Powders. Acta Materialia, 50, 2002, p. 1141.
26 Papparado J. U.S. Navy Finding New Applications for Advances in Nanotechnology. National Defense Industrial Association's Business & Technology Magazine. Available from: http://www.nationaldefensemagazine.org/issues/2004/oct/US_Navy_Finding.htm [accessed 14 December 2006].
27 Williams J., Kim G.E., Walker J. Ball Valves with Nanostructured Titanium Oxide Coatings for High-Pressure Acid-Leach Service: Development to Application. Proceedings of Pressure Hydrometallurgy 2004, Banff, Alberta, Canada, October 23–27, 2004.
28 Kim G.E., Walker J. Successful Application of Nanostructured Titanium Dioxide Coating for High-Pressure Acid-Leach Application. Journal of Thermal Spray Technology, Volume 16(1), March 2007, p. 34.
29 Kim G.E. Thermal Sprayed Nanostructured Coatings: Applications and Developments. Chapter 3 of Nanostructured Materials Processing, Properties, and Applications – 2nd edn, Koch C.C, editor. William Andrew Publishing, 2007.
30 Kim G.E. Proven and Promising Applications of Thermal Sprayed Nanostructured Coatings. Proceedings of the International Thermal Spray Conference, Seattle, USA, May 15–18, 2006.
31 Schoenung J.M., Tang F., Ajdelsztajn L., Kim G.E., Provenzano V. Processing and Characterization of Thermal Barrier Coatings with Cryomilled Bond Coats. Materials Forum, Vol 29, pp. 414–419, 2005.
32 Ajdelsztajn L., Picas J.A., Kim G.E., Bastian F.L., Schoenung J.M., Provenzano V. Oxidation behavior of HVOF sprayed nanocrystalline NiCrAlY powder. Materials Science and Engineering, A338, 2002, p. 33.
33 Ajdelsztajn L., Tang F., Kim G.E., Provenzano V., Schoenung J.M. Synthesis and Oxidation Behavior of Nanocrystalline MCrAlY Bond Coatings. Journal of Thermal Spray Technology, Volume 14(1), March 2005, p. 23.
34 Klug H.P., Alexander L.E., X-Ray Diffraction Procedures: For Polycrystalline and Amorphous Materials, 2nd Edition, New York, NY: Wiley, 1974, p. 643.
35 Suryanarayana C., Mechanical Alloying and Milling, New York, NY: Marcel Dekker, 2004, p. 110.
36 Ur S.C., Choo H., Lee D.B., Nash P. Processing and Properties of Mechanically Alloyed Ni(Fe)Al-Al_2O_3-AlN. Metals and Materials, Vol. 6, No. 5 (2000), p. 435.
37 Dymek S., Dollar M., Hwang S.J., Nash P. Deformation mechanisms and ductility of mechanically alloyed NiAl. Materials Science and Engineering A152 (1992), p. 160.
38 Lee D.B., Kim G.Y., Park S.W., Ur S.C. High temperature oxidation of mechanically alloyed NiAl-Fe-AlN-Al_2O_3. Materials Science and Engineering A329–331 (2002), p. 718.
39 Dollar M., Dymek S., Hwang S.J., Nash P. The Role of Microstructure on Strength and Ductility of Hot-Extruded Mechanically Alloyed NiAl. Metallurgical Transaction A, Volume 24A, September 1993, p. 93.
40 Whittenberger J.D., Eduard A., Luton M.J. 1300 K compressive properties of a reaction milled NiAl-AlN composite. Journal of Materials Research, Volume 5, Issue 12, December 1990, p. 2819.
41 Evans A.G., Mumm D.R., Hutchinson J.W., Meier G.H., Pettit F.S. Mechanism controlling the durability of thermal barrier coatings. Progress in Materials Science, Volume 46, Issue 5, 2001, p. 505.

42 Wright P.K., Evans A.G. Mechanisms governing the performance of thermal barrier coatings. Current Opinion in Solid State and Materials Science, Volume 4, Issue 3, June 1999, p. 255.
43 Wu Y.N., Qin M., Feng Z.C., Liang Y., Sun C., Wang F.H. Improved oxidation resistance of NiCrAlY coatings. Materials Letters 57 (2003), p. 2404.
44 Tang F., Ajdelsztajn L., Kim G.E., Provenzano V., Schoenung J.M. Effects of variations in coating materials and process conditions on the thermal cycle properties of NiCrAlY/YSZ thermal barrier coatings. Mater Sci Eng A425 (2006), p. 94.
45 Mercier D., Kim G.E., Brochu M. Surface Oxide Selectivity of Nanostructured CoNiCrAlY and NiCoCrAlY Materials. Oral presentation at 2009 TMS Annual Meeting & Exhibition, February 15–19, 2009: San Francisco, CA.
46 Kaplin C., Mercier D., Brochu M. Nanostructured MCrAlY Coatings for High Temperature Oxidation in Petrochemical Applications. Oral presentation at Materials Science & Technology 2009, October 25–29, 2009: Pittsburgh, PA.
47 Papyrin A. Cold Spray Technology. Advanced Materials & Processes, September, 2001, p. 49.
48 Van Steenkiste T.H. Kinetic Spray Coatings. Surface and Coatings Technology, 1999, 111, p. 62.
49 Stoltenhoff T., Kreve H., Richter H. An Analysis of the Cold Spray Process and Its Coatings. Journal of Thermal Spray Technology, 2002, Vol. 11(4), p. 542.
50 Dykhuizen R., Smith M. Gas Dynamic Principles of Cold Spray. Journal of Thermal Spray Technology, 1998, 7(2), p. 205.
51 Kosarev V.F., Klinkov S.V., Alkhimov A.P., Papyrin A.N. On Some Aspects of Gas Dynamic Principles of Cold Spray Process. Journal of Thermal Spray Technology, 2003, Vol. 12(2), p. 265.
52 Grujicic M., Zhao C.L., Tong C., DeRosset W.S., Helfritch D. Analysis of the Impact Velocity of Powder Particles in the Cold-Gas Dynamic-Spray Process. Materials Science and Engineering A368, 2004, p. 222.
53 Dykhuizen R.C., Smith M.F., Gilmore D.L., Neiser R.A., Jiang X., Sampath S. Impact of High Velocity Cold Spray Particles. Journal of Thermal Spray Technology, 1999, Vol. 8(4), p. 559.
54 Grujicic M., Saylor J.R., Beasley D.E., Derosset W.S., Helfritch D. Computational Analysis of the Interfacial Bonding between Feed-Powder Particles and the Substrate in the Cold-Gas Dynamic-Spray Process. Applied Surface Science, Vol. 219, 2003, p. 211.
55 Helfritch DJ, Champagne VK. Optimal Particle Size for the Cold Spray Process. Presented at the International Thermal Spray Conference, May, 2006.
56 Champagne V., editor. The Cold Spray Materials Deposition Process: Fundamentals and Applications. Woodhead Publishing Limited, Abington Hall, Abington, Cambridge CB21 6AH, England, 2007, p.57.
57 Grujicic M., Saylor J.R., Beasley D.E., Derosset W.S., Helfritch D. Computational Analysis of the Interfacial Bonding between Feed-Powder Particles and the Substrate in the Cold-Gas Dynamic-Spray Process. Applied Surface Science, Vol. 219, 2003, p. 211.
58 Amateau M.F., Eden T.J. High Velocity Particle Technology. iMast Quarterly, 2000, p. 3.
59 McCune R.C., Donlon W.T., Popoola O.O., Cartwright E.L. Characterization of Copper Layers Produced by Cold Gas-Dynamic Spraying. Journal of Thermal Spray Technology, 2000, Vol. 9(1), p. 73.
60 Moriarty P. Nanostructured Materials. Reports on Progress of Physics, 64 (2001), p. 297.

61 Shukla V., Elliott G.S., Kear B.H. Nanopowder deposition by supersonic rectangular jet impingement. Journal of Thermal Spray Technology, Vol. 9(3), 2000, p. 394.
62 Lima R.S., Karthikeyan J., Kay C.M., Lindemann J., Berndt C.C. Microstructural Characteristics of Cold-Sprayed Nanostructured WC-Co. Thin Solid Films, 416 (2002) p. 129.
63 Kim H.J., Lee C.H., Hwang S.Y. Superhard Nano WC-12%Co Coating by Cold Spray Deposition. Materials Science and Engineering A391 (2005), p. 243.